

Performance Analysis of LEO Satellite-Based IoT Networks in the Presence of Interference

Ayush Kumar Dwivedi¹, *Student Member, IEEE*, Sachin Chaudhari², *Senior Member, IEEE*,
Neeraj Varshney³, *Senior Member, IEEE*, Pramod K. Varshney⁴, *Life Fellow, IEEE*

Abstract—This paper presents a star-of-star topology for internet-of-things (IoT) networks using mega low-Earth-orbit constellations. The proposed topology enables IoT users to broadcast their sensed data to multiple satellites simultaneously over a shared channel, which is then relayed to the ground station (GS) using amplify-and-forward relaying. The GS coherently combines the signals from multiple satellites using maximal ratio combining. To analyze the performance of the proposed topology in the presence of interference, a comprehensive outage probability (OP) analysis is performed, assuming imperfect channel state information at the GS. The paper employs stochastic geometry to model the random locations of satellites, making the analysis general and independent of any specific constellation. Furthermore, the paper examines successive interference cancellation (SIC) and capture model (CM)-based decoding schemes at the GS to mitigate interference. The average OP for the CM-based scheme and the OP of the best user for the SIC scheme are derived analytically. The paper also presents simplified expressions for the OP under a high signal-to-noise ratio (SNR) assumption, which are utilized to optimize the system parameters for achieving a target OP. The simulation results are consistent with the analytical expressions and provide insights into the impact of various system parameters, such as mask angle, altitude, number of satellites, and decoding order. The findings of this study demonstrate that the proposed topology can effectively leverage the benefits of multiple satellites to achieve the desired OP and enable burst transmissions without coordination among IoT users, making it an attractive choice for satellite-based IoT networks.

Index Terms—Amplify-and-forward, LEO satellites, outage probability, satellite-based IoT, stochastic geometry

I. INTRODUCTION

The emerging internet-of-things (IoT) networks aim to connect a large number of devices and sensors over a wide range of applications such as smart cities, e-healthcare, marine IoT, and connected vehicles. Despite significant improvements in terrestrial wireless systems, providing coverage at remote locations remains a challenge, with only 25% of the world's land-mass having terrestrial connectivity [1]. The intrinsic broadcasting capability of satellite systems makes them a viable solution for delivering truly ubiquitous service to IoT networks often deployed remotely over large areas [2]. A recent 3GPP

Rel-17 study-item has also specified the support required for satellite-based NB-IoT/eMTC networks [3]. Recently, many low Earth orbit (LEO) satellite constellations, e.g., Starlink-SpaceX, OneWeb, Kuiper, Telesat, etc., have been launched. They can potentially serve the remotely deployed IoT networks with multiple LEO satellites in the visible range for a large fraction of the Earth's surface [4]. Moreover, they have relatively low propagation delay at lower powers when compared to the legacy geostationary orbit (GEO) satellites.

The previous studies in [5]–[7] have identified several architectural challenges and enabling solutions for satellite-based IoT networks. Specifically, they suggest that upgrades are needed at the physical (PHY) and medium access control (MAC) layers to include non-orthogonal and non-pure ALOHA-based approaches, as well as the exploration of computationally simple random access schemes and novel topologies for massive IoT connectivity. In this paper, we address some of these requirements by proposing a star-of-star topology-based satellite-IoT network. In the past, star topologies have been used in terrestrial low power wide area network (LPWAN) technologies like Sigfox and long range wide area network (LoRaWAN) [8], [9], but their performance has not been explored for satellite-based IoT networks as done in this paper. Unlike previous studies [10]–[12], where either uplink or downlink performance is analyzed for simple channel models, we investigate the end-to-end performance using more realistic channel fading models for satellite communication. We also consider the impact of random access with multiple IoT users transmitting simultaneously as well as the fact that longer distances between IoT users and satellites lead to higher path loss. To address the above factors, we propose a more general system that leverages multiple satellites for improved performance.

Our proposed topology also addresses the energy consumption challenges associated with IoT users, which have limited energy resources. Unlike cellular networks, where significant energy is consumed in listening while in the idle state and in synchronization with the base station for continuous coverage, IoT devices only require intermittent coverage for data transmission. The proposed topology facilitates burst mode of operation that allows IoT devices to transmit data at specific intervals and sleep thereafter, without requiring synchronization and routing. This ensures minimal computational complexity for IoT users and all the processing is shifted to the ground station (GS). The presented results focus on the PHY layer aspects with a particular emphasis on topology and performance analysis.

Ayush Kumar Dwivedi (*Corresponding author*) and Sachin Chaudhari are with the Signal Processing and Communication Research Center at International Institute of Information Technology, Hyderabad 500032, India (e-mail: ayush.dwivedi@research.iiit.ac.in; sachin.c@iiit.ac.in).

Neeraj Varshney is with the Wireless Networks Division, National Institute of Standards and Technology, Gaithersburg, MD 20899 USA (e-mail: neerajv@ieee.org).

Pramod K. Varshney is with the Department of Electrical Engineering and Computer Science, Syracuse University, Syracuse, NY 13244 USA (e-mail: varshney@syr.edu).

TABLE I
COMPARISON OF WORK DONE IN THIS PAPER WITH OTHER PAPERS IN THE LITERATURE

Scope/Reference	[8], [9]	[10], [11]	[12]	[18]	[21]	[29]	[32], [33]	[34]	This paper
Satellite channel model		✓	✓		✓			✓	✓
Direct-access AF topology					✓	✓			✓
Multiple satellites/relays				✓		✓			✓
Interference from other users	✓	✓		✓		✓	✓		✓
Combining at the GS				✓		✓			✓
Random location of satellites		✓					✓	✓	✓
SIC decoding at GS	✓								✓
OP analysis on end-to-end SNR/SINR	✓	✓	✓	✓		✓	✓	✓	✓
Imperfect channel estimates									✓
Asymptotic analysis on SNR			✓	✓	✓	✓			✓
Analysis on effect of system parameters		✓	✓	✓			✓	✓	✓

A. Related Work

In a star-of-star topology, the access between the node and the relay can be direct or indirect, where the satellites can act as a relay/repeater between the node and the server. However, direct-to-satellite IoT (DtS-IoT) has recently gained traction because of its ease of deployment [13]. In [14], it is shown that LPWAN technologies can be configured for realising DtS-IoT communication. Moreover, some manufacturers' low-cost, battery-powered development kits have also provided the impetus to DtS-IoT using LEO satellites [15]–[17]. The feasibility of DtS-IoT has been established by the link budget analysis carried out on IoT users of various power classes by different companies in a recent 3GPP study-item [3].

In DtS-IoT, the satellites can act as regenerative (decode-and-forward (DF)) or transparent (amplify-and-forward (AF)) relays. In [18], the performance of a DF relaying network with randomly distributed interferers is analyzed under Rayleigh and Nakagami- m fading channels. In [19], the performance of selective-DF relaying for DtS-IoT network has been analysed for LEO satellites. But, the complexity of AF relaying with a fixed gain is less than DF relaying [20], and has been preferred in [3]. The performance of topologies employing AF relaying has been widely studied for various systems. For example, in [21], the performance of a hybrid satellite-terrestrial cooperative network consisting of a single AF relay has been analyzed for generalized fading. In [22], [23], [24], and [25], the performance of an AF system with multiple relays and maximal ratio combining (MRC) at the destination has been analysed for Rayleigh, Nakagami- m , Rician, and shadowed-Rician faded channels, respectively. Additionally, co-channel interference has been included in the performance analysis of relay-based topologies in [26], and [27] for Rayleigh and mixed-Rayleigh-Rician fading channels, respectively. However, this interference can be mitigated using various cancellation techniques. In this context, several interference mitigation techniques for both relay and non-relay systems have also been discussed in the literature. A non-orthogonal multiple access (NOMA) inspired system with a single AF relay and a decoding scheme using the signal from two consecutive time slots is analysed in [28]. Similarly a multi-source, multi-relay system with opportunistic interference cancellation using adaptive AF/DF

is analysed in [29]. In both [28] and [29], performance is analysed under the Rayleigh fading assumption. In [8], [9], non-relay terrestrial IoT communication systems have been studied. A LoRaWAN like system with and without fading is considered in [8] and [9], respectively, to show that the capture model (CM) and successive interference cancellation (SIC)-based decoding schemes can perform better than the traditional ALOHA schemes. In CM, the strongest received signal can be decoded successfully despite interference if the signal-to-interference-plus-noise ratio (SINR) is greater than the threshold. Whereas in SIC, decoding is performed in the order of SINRs while cancelling the interference at each step. While NOMA-based IoT network may seem attractive for satellite-based systems as it has more degrees of freedom [30], [31], it is not practical as it will require sophisticated power control algorithms and continuous communication with the ground station, which is not feasible for IoT networks with a large number of devices and limited computational and battery resources.

Recently many mega-LEO constellations have been launched, and more are being proposed for deployment in the near future. For these, performance analysis done using satellite locations based on their orbit simulations can not be generalized for any new constellation in future. Hence, to generalize the analysis for any constellation, tools from stochastic geometry have been used in recent literature where satellites are assumed to be randomly located around the Earth [10], [11], [32]–[34]. In [10], coverage and throughput performance for the uplink of a satellite-based-IoT network has been presented using an empirical channel model representing path-loss and large-scale fading. In [11], a fine-grained analysis has been given for the downlink of a LEO satellites-based mmWave relay network. The satellites are assumed to be uniformly distributed on a spherical cap around the Earth, and meta-distribution of the SINR is used for performance evaluation. In [32], [33], a theoretical analysis of downlink coverage and rate in a LEO constellation is presented. The satellites are modelled as a BPP on a sphere, and the users are located on the Earth's surface. Expressions for statistical characteristics of range and number of visible satellites have been derived along with the notion of an effective number of satellites to suppress

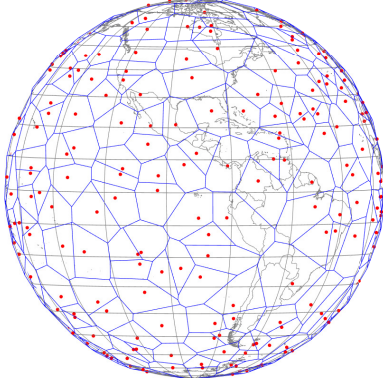


Fig. 1. An example constellation of size $K = 720$ satellites where the satellites are distributed on a spherical surface following a BPP. The Voronoi diagrams represent the area to which the enclosed satellite is the nearest.

the performance mismatch between the practical and random constellations. In [34], the performance of an LEO satellite network with ground-based gateways acting as relays has been compared with a fiber-connected network to demonstrate the coverage gain for rural and remote areas using LEO satellites. In the context of GEO satellites, [12] analyzes the performance of downlink channels for randomly located users in single and multibeam areas.

B. Contributions of the paper

Keeping in mind the requirements of IoT, e.g., simple random access, novel topology, and the results from existing literature, this paper explores a star-of-star topology for satellite-based IoT networks, which can leverage the benefits of multiple satellites in the visible range. The IoT network is envisioned as the subscriber of one of the many services offered by mega-LEO constellations. The satellites are assumed to be randomly distributed as a BPP on a sphere around the Earth such that a user can see a satellite only if its elevation angle is greater than the mask angle. Multiple satellites simultaneously listen to the broadcast information from multiple IoT users and forward it to the GS using fixed-gain AF. It is assumed that IoT users wake up to offload the sensed data to all the visible satellites without any prior coordination and sleep again. This way, the processing is kept simple and energy-efficient for the IoT users, and all the complexity is moved to the satellites and the GS. Since many IoT users are assumed to transmit simultaneously, this work considers CM and SIC-based decoding at the GS.

In [22]–[25], performance analysis was done without considering any interference at the relays as opposed to this paper. Similarly, in [26], [27], although co-channel interference was considered, only a single relay was employed, different from the multiple satellite relay architecture considered in this paper. Neither [9] nor [8] considered a relay system with fading in the propagation environment while analyzing decoding schemes as done in this paper. Moreover, all the above papers neither specifically consider satellites as relays in their performance analysis, nor do they include any information about the location of the sources and relays.

In [10]–[12], [32]–[34], the coverage and rate analysis is limited to only single link (either uplink or downlink)

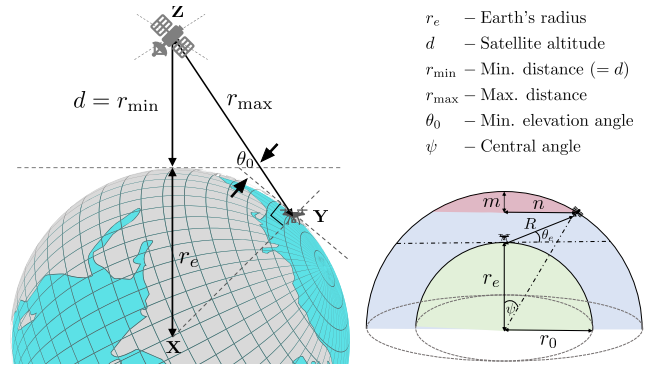


Fig. 2. A geometric representation of the elevation angle θ_e and slant range R between a particular satellite and the IoT user being decoded at GS (maximum slant range r_{\max} is obtained when $\theta_e = \theta_0$).

performance using a single-serving satellite. Also, no mask elevation angle has been considered to define the visibility of a satellite. In our previous preliminary work [35], a similar topology as this paper was employed, but the analysis was limited to scenarios with single-user and no interference. Compared to [35], the analysis in this work is extended to scenarios with multiple interfering users and channels with imperfect knowledge. Also, in [35], all the visible satellites were considered at fixed locations. However, in this work, the performance of the employed topology is analyzed with different decoding schemes using stochastic geometry to generalize the analysis for any LEO satellite constellation. Further, the system parameters like the number of devices, satellites, and mask angle are optimized in this paper to obtain an optimal region of operation. Table I provides a comprehensive comparison of the aspects covered in the key previous works with respect to the aspects covered in this paper.

The specific contributions of this paper are as follows:

- 1) A star-of-star topology is employed for satellite-based IoT networks, which can leverage the benefits of multiple satellites in the visible range.
- 2) The statistical characteristics of the range and the number of visible satellites for a given mask angle are derived in closed form, which is lacking in the existing literature. These characteristics arise from stochastic modelling and are crucial to finding the outage probability (OP).
- 3) The exact expression for the average OP of a user at the GS is derived for CM and the OP for the best user is derived for SIC under the assumption that perfect channel state information (CSI) is not known at the GS. The derived theoretical results are validated with Monte-Carlo simulations.
- 4) Asymptotic expressions of OP under high signal-to-noise ratio (SNR) assumption are obtained, which are much simpler to comprehend and do not include any integrals. The proposed topology is demonstrated to achieve a diversity order equal to the number of satellites used for AF in case of no-interference and perfect CSI. However, the OP attains a floor when there is interference and errors due to imperfect CSI. The asymptotic expressions are further utilized to optimize the system parameters like the

TABLE II
SUMMARY OF SYMBOLS AND NOTATIONS

Symbol	Description	Symbol	Description
U	Number of IoT users	S	Number of satellites used for AF
K	Number of satellites in constellation	K_{vis}	Number of visible satellites
r_e	Radius of Earth (6371 km)	d	Altitude of satellite
R_{us}	Distance between the u^{th} user and s^{th} satellite	R_g	Distance between any satellite and GS
θ_e	Elevation angle	θ_0	Minimum elevation angle or mask angle
P_u	Transmit power of the u^{th} user	P_s	Transmit power of the s^{th} satellite
σ_n^2	AWGN power at satellite for u^{th} user	σ_w^2	AWGN power at GS for s^{th} satellite
\mathcal{R}	Target rate	B	Available bandwidth
h_{us}	Channel coefficient of $(u - s)$ user-satellite pair	g_s	Channel coefficient of s^{th} satellite
m, b, Ω	Parameters of Shadowed Rician channel	γ_{th}	SINR threshold
α	Path loss exponent	P_{out}	Outage probability

number of devices, satellites, and mask angle to obtain the optimal region of operation achieving a target OP.

- 5) The effect of various key design parameters like the number of satellites, altitude, elevation angle and user ordering in SIC on the OP are analyzed.

The rest of the paper is organised as follows: Section II presents the detailed system model, and Section III discusses the statistical characteristics of the range and number of visible satellites. The exact OP derivations for both CM and SIC decoding schemes are derived in Section IV and the asymptotic expressions are derived in Section V. The results and the associated discussions are presented in Section VI, followed by the conclusion in Section VII.

II. SYSTEM DESCRIPTION

As shown in Fig. 1, a total of K satellites are assumed to be distributed uniformly around the Earth at an altitude d km such that they form a BPP on a sphere of radius $r_e + d$, where r_e is the radius of the Earth. The users are assumed to be located on the Earth's surface. A satellite is considered visible and can receive a signal from a user only if its elevation angle θ_e w.r.t user's location is greater than a minimum elevation or mask angle θ_0 —any satellite for which $\theta_e < \theta_0$ is considered invisible to the user. As shown in Fig. 2, the distance between a user and a satellite will be minimum when the satellite is at maximum elevation $\theta_e = 90^\circ$ w.r.t the user. This minimum distance r_{min} equals the altitude d at which all the satellites in the constellation are deployed. Similarly, the distance between a user and a satellite is maximum when the satellite is at an elevation angle $\theta_e = \theta_0$ w.r.t to the user. The maximum distance for a fixed θ_0 can be derived as shown in Appendix A. All the notations followed in this paper are defined in Table II.

As shown in Fig. 3, a direct access topology based on a mega-LEO constellation is explored, where U IoT users communicate their sensed information to a GS via S satellites among all the K_{vis} visible-satellites. The IoT users are assumed to broadcast their information simultaneously using shared resources at the start of every slot as per the slotted-ALOHA scheme similar to the case shown in [36]. Keeping in mind the low complexity of IoT users and design for a common application, it is assumed that all the users transmit at equal power.

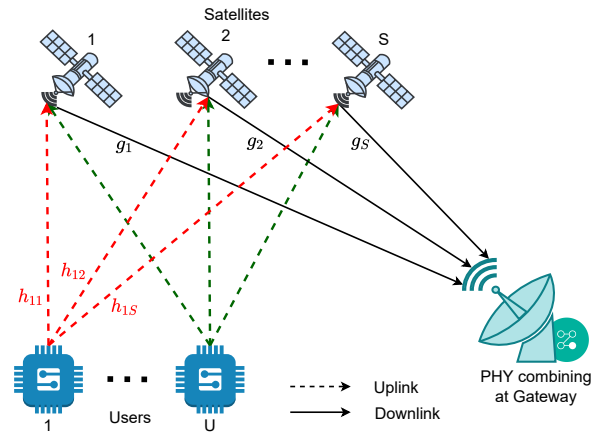


Fig. 3. Schematic diagram of the proposed topology with U IoT users broadcasting their sensed information to S visible satellites simultaneously (different colours are used to indicate transmissions from each user). All the satellites forward the signals to the GS using fixed-gain AF relaying.

The visible satellites amplify and re-transmit the received information to the GS. The GS decodes the information of all the users after coherently combining the signals received from all satellites. Thus, end-to-end communication takes place in two phases. In the first phase, all the IoT users who have sensed information broadcast their signal to all the satellites in the visible range. The signal received at the s^{th} satellite can be written as

$$y_s = \sum_{u=1}^U \sqrt{P_u \mathcal{G}_u \mathcal{G}_s(\varphi_{us}) (\lambda/4\pi r_{us})^\alpha} (\hat{h}_{us} + e_{us}) x_u + n_s, \quad (1)$$

where P_u is the transmit power of the u^{th} IoT user, r_{us} is the distance between the u^{th} user and the s^{th} satellite, α is the path loss exponent, x_u is the unit energy information signal, n_s is the additive white Gaussian noise (AWGN) with zero mean and variance σ_n^2 at the satellite receiver, \hat{h}_{us} is the shadowed-Rician (SR) distributed imperfect estimate of the channel coefficient and e_{us} is the estimation error. Similar to the approach followed in [37]–[40], the estimation error e is considered to be distributed as $\mathcal{CN}(0, \sigma_e^2)$ with an SNR dependent variance $\sigma_e^2 = \phi \eta^{-\chi}$, where ϕ and χ are deterministic constants. Here, a perfect CSI can be obtained if

$$\begin{aligned} \gamma_{us} &= \frac{r_{\min}^{-\alpha} r_{us}^{-\alpha} G_s H_{us}}{r_{\min}^{-\alpha} G_s \left(\sum_{\substack{i=1 \\ i \neq u}}^U r_{is}^{-\alpha} H_{is} + \sum_{u=1}^U \eta_u r_{us}^{-\alpha} \sigma_{e_{us}}^2 + 1 \right) + \eta_s \sigma_{e_s}^2 r_{\min}^{-\alpha} \left(\sum_{u=1}^U r_{us}^{-\alpha} (H_{us} + \eta_u \sigma_{e_{us}}^2) + 1 \right) + \frac{P_s}{\beta_{\text{AF}}^2 \sigma_n^2}}, \\ &= \frac{r_{us}^{-\alpha} G_s H_{us}}{G_s \left(\sum_{\substack{i=1 \\ i \neq u}}^U r_{is}^{-\alpha} H_{is} + \sum_{u=1}^U \eta_u r_{us}^{-\alpha} \sigma_{e_{us}}^2 + 1 \right) + \eta_s \sigma_{e_s}^2 \left(\sum_{u=1}^U r_{us}^{-\alpha} (H_{us} + \eta_u \sigma_{e_{us}}^2) + 1 \right) + \hat{C}}, \end{aligned} \quad (6)$$

$\chi \rightarrow \infty$ for $\eta > 0$. The transmit and the receive antenna gains at the user and the satellite are denoted as \mathcal{G}_u and $\mathcal{G}_s(\varphi_{us})$ respectively, where φ_{us} is the angle between the u^{th} user location and the beam center with respect to the s^{th} satellite.

The SR model best characterizes the channels which experience line-of-sight (LoS) shadowing and small-scale fading [41]. It is a generalized form of a Rician fading model where the LoS component is assumed to undergo Nakagami- m fading. The SR model is known to fit best the experimental data in the case of characterizing satellite models [41]. For any SR random variable h_i , the probability density function (PDF) and cumulative distribution function (CDF) of $H_i = \eta_i |h_i|^2$, are given, respectively in [42] by

$$\begin{aligned} f_{H_i}(x) &= \alpha_i \sum_{\kappa=0}^{m_i-1} \frac{\zeta(\kappa)}{\eta_i^{\kappa+1}} x^\kappa e^{-\left(\frac{\beta_i - \delta_i}{\eta_i}\right)x}, \\ F_{H_i}(x) &= 1 - \alpha_i \sum_{\kappa=0}^{m_i-1} \frac{\zeta(\kappa)}{\eta_i^{\kappa+1}} \sum_{p=0}^{\kappa} \frac{\kappa!}{p!} \left(\frac{\beta_i - \delta_i}{\eta_i}\right)^{-(\kappa+1-p)} \\ &\quad \times x^p e^{-\left(\frac{\beta_i - \delta_i}{\eta_i}\right)x}, \end{aligned} \quad (2)$$

where $\alpha_i = ((2b_i m_i)/(2b_i m_i + \Omega_i))^{m_i} / 2b_i$, $\beta_i = 1/2b_i$, $\delta_i = \Omega_i / (2b_i(2b_i m_i + \Omega_i))$ and $\zeta(\kappa) = (-1)^\kappa (1 - m_i)_\kappa \delta_i^\kappa / (\kappa!)^2$ with $(\cdot)_\kappa$ being the Pochhammer symbol [43]. Here $2b_i$ denotes the average power of the multipath component, and Ω_i is the average power of the LoS component. The LEO satellites also observe Doppler shifts, but it has not been considered here to keep the analysis simple. It is assumed that the Doppler can be compensated using known techniques [44].

In the second phase, the satellites employ AF to send the received signals to the GS using dedicated orthogonal resources without interference. This assumption considers the downlink between the satellites and GS to be resource sufficient. Moreover, it keeps the analysis simpler and focused on the effect of uplink, which is limited by the transmit power of the IoT users. Similar to the store-and-forward scheme adopted in [15], it is considered that satellites offload their information when they are nearest to the GS within a time range, i.e. $r_g = r_{\min}$. The S satellites among the K_{vis} visible satellites which offload their information to the GS in the defined time range are considered for MRC. The received signal from the s^{th} satellite at the GS can be written as

$$z_s = \beta_{\text{AF}} \sqrt{G_s \mathcal{G}_{\text{GS}}(\varphi_s) (\lambda/4\pi r_{\min})^\alpha} (\hat{g}_s + e_s) y_s + w_s, \quad (4)$$

where \hat{g}_s is the estimated SR channel coefficient between the

s^{th} satellite and GS, e_s is the estimation error distributed as $\mathcal{CN}(0, \sigma_{e_s}^2)$, β_{AF} is the AF gain factor and w_s is the additive white Gaussian noise with zero mean and variance σ_w^2 at the GS receiver. The transmit and the receive antenna gains at the satellite and the GS are denoted as \mathcal{G}_s and $\mathcal{G}_{\text{GS}}(\varphi_s)$ where φ_s is the angle between the s^{th} satellite location and the beam center with respect to the GS. Ideally, the effect of the channel between the user and the satellite is equalized by the AF gain factor [20]. In this paper, the received signal is scaled at the satellite by a fixed-gain factor β_{AF} , which is inversely proportional to the total received power and is defined as

$$\beta_{\text{AF}} = \sqrt{\frac{P_s}{\sum_{u=1}^U P_u \mathcal{G}_u \mathcal{G}_s(\varphi_{us}) \left(\frac{\lambda}{4\pi}\right)^\alpha \mathbb{E} \left[r_{us}^{-\alpha} (|\hat{h}_{us}|^2 + \sigma_{e_{us}}^2) \right] + \sigma_n^2}}. \quad (5)$$

The instantaneous end-to-end SINR of the information signal from the s^{th} satellite for the u^{th} user at the GS can be written as (6), where $H_{us} = \eta_u |\hat{h}_{us}|^2$ is the instantaneous SNR of a user-satellite link with $\eta_u = \frac{P_u}{\sigma_n^2} \mathcal{G}_u \mathcal{G}_s(\varphi_{us}) (\lambda/4\pi)^\alpha$, $G_s = \eta_s |\hat{g}_s|^2$ is the instantaneous SNR of a satellite-GS link with $\eta_s = \frac{P_s}{\sigma_w^2} \mathcal{G}_s \mathcal{G}_{\text{GS}}(\varphi_s) (\lambda/4\pi)^\alpha$ and $\hat{C} = \frac{P_s}{r_{\min}^{-\alpha} \sigma_n^2 \beta_{\text{AF}}^2}$. Using (5), we can further simplify \hat{C} as

$$\hat{C} = \frac{1}{r_{\min}^{-\alpha}} \left\{ 1 + \sum_{u=1}^U (\mathbb{E} [r_{us}^{-\alpha} H_{us}] + \eta_u \sigma_{e_{us}}^2 \mathbb{E} [r_{us}^{-\alpha}]) \right\}. \quad (7)$$

Since the GS combines the signals from all the visible satellites using MRC, the end-to-end SINR of the combined signal for the u^{th} user at the GS is given by

$$\gamma_u = \sum_{s=1}^S \gamma_{us}. \quad (8)$$

In this paper, two decoding schemes are compared to analyse the performance of the proposed topology:

- *Capture model (CM)*: The GS is assumed to perfectly decode the information of the desired user out of many interfering signals if its SINR is higher than a threshold. This type of decoding is similar to the capture effect used in LoRa [45].
- *Successive interference cancellation (SIC)*: The GS decodes the information of the intended user by successively removing the information of other users in the order of

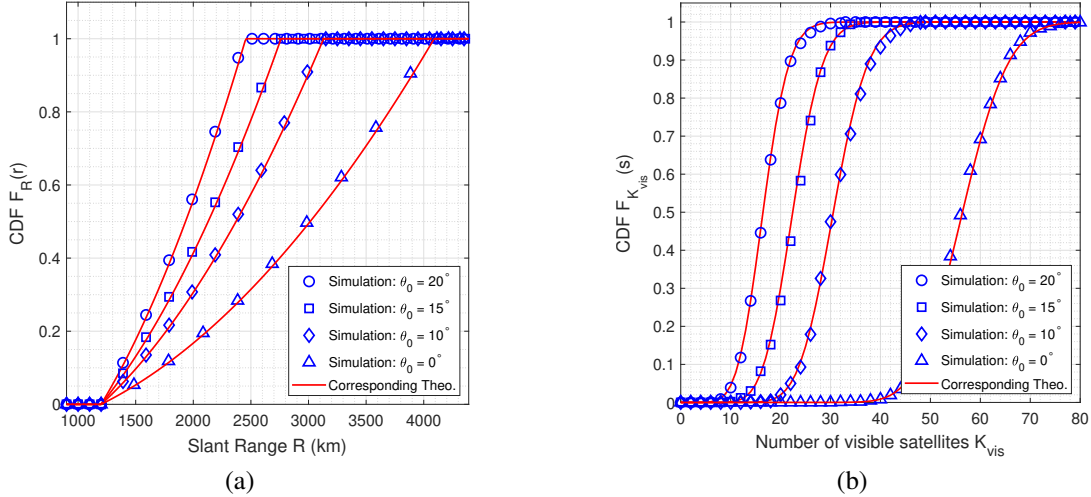


Fig. 4. (a) CDF $F_R(r)$ of the distance between a user and a visible satellite in the constellation at 1200 km altitude. (b) CDF $F_{K_{vis}}(s)$ of the number of satellites visible to any user in a constellation of 720 satellites at 1200 km altitude.

their SINRs [46]. The user with the highest SINR is decoded first, and its reconstructed signal is subtracted from the received superimposed signal to decode the remaining users. However, even after removing the interference, there may still be some residual error remaining due to noise or imperfect decoding. The user with SINR less than the threshold and subsequent users in the order are considered non-decodable and contribute to the outage.

III. SLANT DISTANCE AND THE NUMBER OF VISIBLE SATELLITES

Since the satellites are considered to be distributed on a spherical surface following a BPP, the distance between a user and a satellite is random. Moreover, the total number of visible satellites is also random and depends upon θ_0 and the total number of satellites in the constellation K . Statistical characteristics of the slant distance and number of visible satellites are derived in this section.

A. Statistical characteristics of the distance between the user and the satellite

The CDF of the distance R between a user and visible satellites in the constellation is given by

$$F_R(r) = \begin{cases} 0, & r < r_{\min} \\ \frac{r^2 - r_{\min}^2}{r_{\max}(\theta_0)^2 - r_{\min}^2}, & r_{\min} \leq r \leq r_{\max}(\theta_0) \\ 1, & r > r_{\max}, \end{cases} \quad (9)$$

and the corresponding PDF is given by

$$f_R(r) = \begin{cases} \frac{2r}{r_{\max}(\theta_0)^2 - r_{\min}^2}, & r_{\min} \leq r \leq r_{\max}(\theta_0) \\ 0, & \text{otherwise,} \end{cases} \quad (10)$$

where $r_{\min} = d$ is the orbital altitude and $r_{\max}(\theta_0) = \sqrt{(r_e \sin \theta_0)^2 + (r_e + r_{\min})^2} - r_e \sin \theta_0$ is the maximum distance observed at mask elevation angle θ_0 . The proofs for (9) and (10) are provided in Appendix A. The effect of θ_0 on the range can be inferred from Fig. 4a. It can be observed that the derived expressions match the simulation results. The slant range for which the CDF reaches 1 corresponds to the maximum possible range for a user. As the mask angle increases, the maximum possible range decreases. However, it can be observed that the maximum range decreases rapidly with an increase in the mask angle from 0° to 10° when compared to 10° to 20° . It can be attributed to the fact that, r_{\max} changes non-linearly with change in θ_0 as shown in (50).

Remark: For the special case of $\theta_0 = 0^\circ$, $r_{\max}(0^\circ) = \sqrt{r_{\min}^2 + 2r_e r_{\min}}$. Hence for $r_{\min} \leq r \leq r_{\max}(0^\circ)$, (9) and (10) can be simplified as

$$F_{R_0}(r) = \frac{r^2 - r_{\min}^2}{2r_e r_{\min}}, \quad (11)$$

$$f_{R_0}(r) = \frac{r}{r_e r_{\min}}, \quad (12)$$

where R_0 denotes the random variable for R at $\theta_0 = 0^\circ$. The expressions in (11) and (12) match with the expressions given for the characteristics of the distance in [11], where they are derived for $\theta_0 = 0^\circ$ only. The simplified expressions shown above are used for scenarios where high-rise structures like mountains and buildings do not mask satellite visibility.

B. Statistical characteristics of the number of visible satellites

A satellite is visible to a user only if its elevation angle exceeds the minimum required elevation θ_0 , also called the mask angle. For a given mask elevation angle θ_0 , the number of visible satellites K_{vis} to any user is a binomial random variable with success probability

$$\mathcal{P} = \frac{r_{\max}(\theta_0)^2 - r_{\min}^2}{4r_e(r_e + r_{\min})}, \quad (13)$$

$$F_{\gamma_{us} | r_{us}}(x) = 1 - \sum_{k_1=0}^{m_{us}-1} \sum_{p=0}^{k_1} \alpha_{us} \frac{k_1! \zeta(k_1)}{p! \eta_{us}^{k_1+1}} A_1^{-(k_1+1-p)} \sum_{k_2=0}^{m_s-1} \alpha_s \frac{\zeta(k_2)}{\eta_s^{k_2+1}} \sum_{z=0}^p \binom{p}{z} \left(\frac{x a}{r_{us}^{-\alpha}} \right)^{p-z} \exp \left[-A_1 \left(\frac{x a}{r_{us}^{-\alpha}} \right) \right] \left(\frac{x C}{r_{us}^{-\alpha}} \right)^z \times \int_{g=0}^{\infty} g^{-z+k_2} \exp \left[-A_1 \left(\frac{x C}{r_{us}^{-\alpha} g} \right) - A_2 g \right] dg, \quad (18)$$

$$F_{\gamma_{us} | r_{us}}(x) = 1 - \sum_{k_1=0}^{m_{us}-1} \sum_{p=0}^{k_1} \alpha_{us} \frac{k_1! \zeta(k_1)}{p! \eta_{us}^{k_1+1}} A_1^{-(k_1+1-p)} \sum_{k_2=0}^{m_s-1} \alpha_s \frac{\zeta(k_2)}{\eta_s^{k_2+1}} \sum_{z=0}^p \binom{p}{z} \left(\frac{x a}{r_{us}^{-\alpha}} \right)^{p-z} \exp \left[-A_1 \left(\frac{x a}{r_{us}^{-\alpha}} \right) \right] \left(\frac{x C}{r_{us}^{-\alpha}} \right)^z \times 2 \left(\frac{A_1 x C}{A_2 r_{us}^{-\alpha}} \right)^{(1-z+k_2)/2} K_{1-z+k_2} \left(2 \sqrt{\frac{A_1 A_2 x C}{r_{us}^{-\alpha}}} \right), \quad (19)$$

where $r_{\max}(\theta_0)$ is the distance observed at θ_0 . The proof for (13) is provided in Appendix B. The effect of mask angle on the number of visible satellites can be inferred from Fig. 4b. It can be observed that the derived expressions match the simulation results. The number of visible satellites for which CDF equals 1 denotes the maximum possible number of satellites which can be visible to a user. As the mask angle increases, the surface area of the cap region shown in Fig. 2 decreases, and so does the maximum number of visible satellites. It can be observed that the maximum possible number of visible satellites decreases rapidly from 0° to 10° when compared to 10° to 20° . It can be understood using (50) and (56), since A_{vis} decreases non-linearly with an increase in θ_e .

Remark: With \mathcal{P}_0 denoting the success probability for the special case of $\theta_0 = 0^\circ$, (13) can be simplified as

$$\mathcal{P}_0 = \frac{r_{\min}}{2(r_e + r_{\min})}. \quad (14)$$

IV. OUTAGE PROBABILITY ANALYSIS

The outage probability of a particular user is defined as

$$P_{\text{out}}(\mathcal{R}) \triangleq \mathbb{P} \left[\frac{B}{2} \log_2(1 + \text{SINR}) \leq \mathcal{R} \right] = \mathbb{P}[\text{SINR} \leq \gamma_{\text{th}}], \quad (15)$$

where \mathcal{R} is the target rate, B is the bandwidth, $\gamma_{\text{th}} \triangleq 2^{2\mathcal{R}/B} - 1$ is the threshold and SINR needs to be calculated for CM and SIC schemes separately.

A. OP for CM based decoding

In CM based decoding, a user is decoded in the presence of interference from all other users. Hence the OP of a user at the GS can be written as

$$P_{\text{out}}(\mathcal{R}) = (\mathbb{P}[\gamma_u \leq \gamma_{\text{th}}] \times \mathbb{P}[K_{\text{vis}} \geq S]) + \mathbb{P}[K_{\text{vis}} < S] = (F_{\gamma_u}(\gamma_{\text{th}}) \times \mathbb{P}[K_{\text{vis}} \geq S]) + \mathbb{P}[K_{\text{vis}} < S], \quad (16)$$

where $\gamma_u = \sum_{s=1}^S \gamma_{us}$ and $\mathbb{P}[K_{\text{vis}} \geq S] = 1 - \sum_{j=0}^{S-1} \binom{K}{j} \mathcal{P}^j (1 - \mathcal{P})^{K-j}$. The following three-step approach has been followed to find the exact expression for (16).

- 1) Finding the CDF of γ_{us} conditioned on r_{us} for a single satellite scenario.

- 2) Finding the moment generating function (MGF) of γ_{us} and γ_u for extending the analysis to the multi-satellite scenario.
- 3) Finding the CDF of γ_u and consequently the OP in multi-satellite scenario.

Step 1: Using the theorem of transformation of random variables, the CDF of γ_{us} conditioned on the distance between the user and the satellite can be found as

$$F_{\gamma_{us} | r_{us}}(x) = \mathbb{P}[\gamma_{us} \leq x | r_{us}] \stackrel{(i)}{\approx} \mathbb{P} \left[\frac{r_{us}^{-\alpha} G_s H_{us}}{G_s ((U-1)\bar{I} + U\bar{E}_1 + 1) + \bar{E}_2 + \hat{C}} \leq x \mid r_{us} \right] \stackrel{(ii)}{=} \int_{g=0}^{\infty} F_{H_{us}} \left(\frac{x a}{r_{us}^{-\alpha}} + \frac{x C}{r_{us}^{-\alpha} g} \right) f_{G_s}(g) dg, \quad (17)$$

where in (i), interference for a user and error terms due to CSI mismatch are approximated as $\bar{I} = \mathbb{E}[r_{is}^{-\alpha} H_{is}]$, $\bar{E}_1 = \eta_u \sigma_{e_{us}}^2 \mathbb{E}[r_{is}^{-\alpha}]$ and $\bar{E}_2 = \eta_s \sigma_{e_s}^2 U (\bar{I} + \bar{E}_1)$ for mathematical tractability and in (ii), $a = (U-1)\bar{I} + U\bar{E}_1 + 1$ and $C = \bar{E}_2 + \hat{C}$ for convenience. The expressions for the terms $\mathbb{E}[r_{is}^{-\alpha}]$ and $\mathbb{E}[r_{is}^{-\alpha} H_{is}]$ are derived in Appendix C. Using (2), (3), with the knowledge of binomial expansion and interchanging the order of summation and integration, (17) can be simplified as (18), where $A_1 = \frac{\beta_{us} - \delta_{us}}{\eta_{us}}$ for uplink and $A_2 = \frac{\beta_s - \delta_s}{\eta_s}$ for downlink. The integral expression in (18) can be solved using [43, Eq. 3.471.9] to get the closed-form expression for $F_{\gamma_{us} | r_{us}}(x)$ as shown in (19), where $K_v(\cdot)$ is the v^{th} order modified Bessel function of second kind.

Step 2: For any random variable X , with MGF $M_X(t)$ and $\mathcal{L}\{\cdot\}$ denoting the Laplace transform operator, we can write

$$\mathcal{L}\{f_X(x)\} = M_X(-t), \quad \mathcal{L}\{F_X(x)\} = \frac{M_X(-t)}{t}, \quad (20)$$

where (20) follows from the integral property of Laplace transform. Therefore, flipped MGF, $M_X(-t)$ is required to obtain CDF by applying the inverse Laplace transform on (20). The flipped MGF (referred simply as MGF hereafter) of γ_{us} conditioned on r_{us} can be derived using the definition of the

$$\begin{aligned}
M_{\gamma_{us} | r_{us}}(-t) &= 1 - t \sum_{k_1=0}^{m_{us}-1} \sum_{p=0}^{k_1} \alpha_{us} \frac{k_1! \zeta(k_1)}{p! \eta_{us}^{k_1+1}} A_1^{-(k_1+1-p)} \sum_{k_2=0}^{m_s-1} \alpha_s \frac{\zeta(k_2)}{\eta_s^{k_2+1}} \sum_{z=0}^p \binom{p}{z} (a r_{us}^\alpha)^{p-z} (C r_{us}^\alpha)^{(1+z+k_2)/2} \\
&\quad \times \left(\frac{A_1}{A_2} \right)^{(1-z+k_2)/2} \epsilon^{-\mu} \exp \left[\frac{\Lambda^2}{2\epsilon} \right] \frac{\Gamma(\mu + \nu + \frac{1}{2}) \Gamma(\mu - \nu + \frac{1}{2})}{\Lambda} W_{-\mu, \nu} \left(\frac{\Lambda^2}{\epsilon} \right), \quad (22)
\end{aligned}$$

Laplace transform as

$$M_{\gamma_{us} | r_{us}}(-t) = 1 - t \int_{x=0}^{\infty} e^{-tx} (1 - F_{\gamma_{us} | r_{us}}(x)) dx. \quad (21)$$

Using (19) and [43, Eq. 6.643.3], the integral in (21) can be solved to arrive at the closed-form expression for $M_{\gamma_{us} | r_{us}}(-t)$ as shown in (22), where

$$\begin{aligned}
\mu &= p + 1 + \frac{k_2 - z}{2}, \\
\epsilon &= A_1 a r_{us}^\alpha + t, \\
\Lambda &= \sqrt{A_1 A_2 C r_{us}^\alpha}, \\
\nu &= \frac{1 - z + k_2}{2},
\end{aligned}$$

and $\Gamma(\cdot)$, $W_{\mu, \nu}(\cdot)$ are the Gamma and Whittaker functions, respectively.

The MGF of γ_{us} can be calculated by averaging over r_{us} using (10) and (22) as

$$\begin{aligned}
M_{\gamma_{us}}(-t) &= \int_{r_{\min}}^{r_{\max}} M_{\gamma_{us} | r_{us}}(-t) f_R(r_{us}) dr_{us} \\
&= \frac{2}{r_{\max}^2 - r_{\min}^2} \int_{r_{\min}}^{r_{\max}} r_{us} M_{\gamma_{us} | r_{us}}(-t) dr_{us}. \quad (23)
\end{aligned}$$

The integral in (23) can be efficiently evaluated using numerical techniques as discussed in Appendix D.

The MRC is implemented at the GS on the signal with end-to-end SINR as defined in (8). Since all the S satellite-GS links are independent, the MGF of the end-to-end SINR can be written as

$$M_{\gamma_u}(-t) = \prod_{s=1}^S M_{\gamma_{us}}(-t). \quad (24)$$

Step 3: Using (20), the CDF of γ_u as be obtained as

$$F_{\gamma_u}(x) = \mathcal{L}^{-1} \left\{ \frac{M_{\gamma_u}(-t)}{t} \right\} (x). \quad (25)$$

The inverse Laplace transform in (25) can be efficiently calculated using the numerical technique presented in [47] as

$$\begin{aligned}
F_{\gamma_u}(x) &= \frac{2^{-Q} e^{D/2}}{x} \sum_{q=0}^Q \binom{Q}{q} \\
&\quad \sum_{n=0}^{N+q} \frac{(-1)^n}{\Delta_n} \Re \left\{ \frac{M_{\gamma_u} \left(-\frac{D + 2\pi j n}{2x} \right)}{\frac{D + 2\pi j n}{2x}} \right\} \\
&\quad + E(D, Q, N), \quad (26)
\end{aligned}$$

where

$$\Delta_n = \begin{cases} 2, & n = 0 \\ 1, & n = 1, 2, \dots, N \end{cases}$$

and

$$\begin{aligned}
E(D, Q, N) &= \frac{e^{-D}}{1 - e^{-D}} + \frac{2^{-Q} e^{D/2}}{x} \sum_{q=0}^Q (-1)^{N+1+q} \binom{Q}{q} \\
&\quad \Re \left\{ \frac{M_{\gamma_u} \left(-\frac{D + 2\pi j (N + q + 1)}{2x} \right)}{\frac{D + 2\pi j (N + q + 1)}{2x}} \right\}.
\end{aligned}$$

The values of D , Q and N are selected to keep the discretization and truncation errors negligible. Thus, using (13) and (26) in (16), completes the derivation of OP for CM-based decoding.

B. OP for SIC based decoding

SIC is an ordering-based scheme where the GS decodes the information of users in the order of their end-to-end SINRs. The residual error due to imperfect interference cancellation is considered to be distributed as $\mathcal{CN}(0, \xi)$ where ξ represents the power of the residual error. For the ease of understanding, $l \in [1, U]$ is used to denote the order/iteration of SIC decoding and $\mathbf{D}[l]$ is used to denote the set of indexes for all decoded users till the l^{th} iteration. Additionally, $\mathbf{D}\{l\}$ is used to denote the index of the user decoded at the l^{th} iteration. Therefore end-to-end SINR of the signal from u^{th} user received via s^{th} satellite in the l^{th} iteration of SIC decoding can be written as

$$\begin{aligned}
\gamma_{us}^{(l)} &= \frac{r_{us}^{-\alpha} G_s H_{us}}{G_s ((U-l)\bar{I} + U\bar{E}_1 + (l-1)\bar{E}_3 + 1) + \bar{E}_2 + \bar{C}} \\
&\quad \forall u \notin \mathbf{D}[l-1], \quad (27)
\end{aligned}$$

where $\bar{E}_3 = \eta_u \xi \mathbb{E}[r_{is}^{-\alpha}]$. Also, the end-to-end SINR of the MRC combined signal of the u^{th} user can be written as

$$\gamma_u^{(l)} = \sum_{s=1}^S \gamma_{us}^{(l)} \quad \forall u \notin \mathbf{D}[l-1]. \quad (28)$$

At every iteration, the user with the highest SINR is decoded such that

$$\gamma_{\mathbf{D}\{l\}}^{(l)} = \begin{cases} \max_u \gamma_u^{(l)}, & l = 1 \\ \max_{u, u \notin \mathbf{D}[l-1]} \gamma_u^{(l)}, & \gamma_{\mathbf{D}\{l-1\}}^{(l-1)} > \gamma_{\text{th}}, l > 1 \\ 0, & \text{otherwise,} \end{cases} \quad (29)$$

$$F_{\tilde{H}_{us}}(z) = \int_{r_{\min}}^{r_{\max}} F_{H_{us}}\left(\frac{z}{r_{us}^\alpha}\right) f_R(r_{us}) dr_{us} = 1 - \frac{2\alpha_{us}}{r_{\max}^2 - r_{\min}^2} \sum_{k=0}^{m_{us}-1} \sum_{p=0}^k \frac{k! \zeta(k)}{p! \eta_{us}^{k+1}} A^{-(k+1-p)} \int_{r_{\min}}^{r_{\max}} (z r_{us}^\alpha)^p \exp[-Az r_{us}^\alpha] r_{us} dr_{us}, \quad (34)$$

$$F_{\tilde{H}_{us}}(z) = 1 - \frac{2}{r_{\max}^2 - r_{\min}^2} \sum_{k=0}^{m_{us}-1} \sum_{p=0}^k \alpha_{us} \frac{k! \zeta(k)}{p! \eta_{us}^{k+1}} A^{-(k+1-p)} \left(\frac{\gamma(V, \rho r_{\max}^\alpha) - \gamma(V, \rho r_{\min}^\alpha)}{\alpha \rho^V} \right) z^p. \quad (35)$$

$$M_{\gamma_{us}^{(1)}|G_s}(-t) = 1 - \frac{2t}{r_{\max}^2 - r_{\min}^2} \sum_{k=0}^{m_{us}-1} \sum_{p=0}^k \frac{\alpha_{us}}{\alpha} \frac{k! \zeta(k)}{p! \eta_{us}^{k+1}} A^{-(k-p+V+1)} \left(a + \frac{C}{g_s}\right)^{p-V} \times \int_{x=0}^{\infty} e^{-tx} x^{p-V} \left\{ \gamma\left(V, A r_{\max}^\alpha \left(a + \frac{C}{g_s}\right) x\right) - \gamma\left(V, A r_{\min}^\alpha \left(a + \frac{C}{g_s}\right) x\right) \right\} dx. \quad (37)$$

$$M_{\gamma_{us}^{(1)}|G_s}(-t) = 1 - \frac{2t}{r_{\max}^2 - r_{\min}^2} \sum_{k=0}^{m_{us}-1} \sum_{p=0}^k \frac{\alpha_{us}}{\alpha} \frac{k! \zeta(k)}{p! \eta_{us}^{k+1}} A^{-(k-p+V+1)} \left(a + \frac{C}{g_s}\right)^{p-V} \frac{\Gamma(p+1)}{V} \times \left\{ \frac{[v_1(g_s)]^V}{[v_1(g_s) + t]^{p+1}} {}_2F_1\left(1, p+1; V+1; \frac{v_1(g_s)}{v_1(g_s) + t}\right) - \frac{[v_2(g_s)]^V}{[v_2(g_s) + t]^{p+1}} {}_2F_1\left(1, p+1; V+1; \frac{v_2(g_s)}{v_2(g_s) + t}\right) \right\}, \quad (38)$$

where the set of indexes for all the decoded users is updated after every iteration as

$$\mathbf{D}[l-1] = \begin{cases} \emptyset, & l = 1 \\ \mathbf{D}[l-2] \cup \{\arg \max_{u, u \notin \mathbf{D}[l-2]} \gamma_u^{(l-1)}\}, & \gamma_{\mathbf{D}[l-1]}^{(l-1)} > \gamma_{\text{th}}, l > 1 \\ \mathbf{D}[l-2], & \gamma_{\mathbf{D}[l-1]}^{(l-1)} \leq \gamma_{\text{th}}, l > 1. \end{cases} \quad (30)$$

Therefore the OP of l^{th} user in case of SIC can be written as

$$P_{\text{out}}^{(l)}(\mathcal{R}) = \begin{cases} \left(\mathbb{P}[\max_u \gamma_u^{(l)} \leq \gamma_{\text{th}}] \mathbb{P}[K_{\text{vis}} \geq S] \right) + \mathbb{P}[K_{\text{vis}} < S], & l = 1 \\ \left\{ \mathbb{P}[\gamma_{\mathbf{D}\{l\}}^{(l)} \leq \gamma_{\text{th}} | \gamma_{\mathbf{D}\{l-1\}}^{(l-1)} > \gamma_{\text{th}}] (1 - P_{\text{out}}^{(l-1)}(\mathcal{R})) \right. \\ \left. + P_{\text{out}}^{(l-1)}(\mathcal{R}) \right\} \mathbb{P}[K_{\text{vis}} \geq S] + \mathbb{P}[K_{\text{vis}} < S], & l > 1, \end{cases} \quad (31)$$

or simply as

$$P_{\text{out}}^{(l)}(\mathcal{R}) = \left(F_{\gamma_u^{(l)}}(\gamma_{\text{th}}) \times \mathbb{P}[K_{\text{vis}} \geq S] \right) + \mathbb{P}[K_{\text{vis}} < S]. \quad (32)$$

The exact expression of (32) for $l = 1$ can be obtained. However, for $l > 1$ it is not mathematically tractable since the distribution of $\gamma_{\mathbf{D}\{l\}}^{(l)}$ conditioned on $\gamma_{\mathbf{D}\{l-1\}}^{(l-1)} > \gamma_{\text{th}}$ is difficult to obtain. Therefore, the exact expression for OP in case of SIC is obtained for the best user ($l = 1$) only, which is a lower bound on the average OP of the system and simulation results are presented for $l > 1$. For the case of $l = 1$, distribution for maximum of dependent random variables $\gamma_u^{(1)}$ is required. Hence the derivation is done using the following steps:

1) Finding the CDF of $\gamma_{us}^{(1)}$ conditioned on G_s for single

satellite scenario.

- 2) Finding the MGF of $\gamma_{us}^{(1)}$ and $\gamma_u^{(1)}$ conditioned on G_s for extending the analysis to multi-satellite scenario.
- 3) Finding the CDF and consequently the OP for $\max_u \gamma_u^{(1)}$ averaged over all G_s .

Step 1: Using the theorem of transformation of random variables, the CDF of $\gamma_{us}^{(1)}$ conditioned on G_s can be written as:

$$F_{\gamma_{us}^{(1)}|G_s} = \mathbb{P}\left[\frac{r_{us}^{-\alpha} G_s H_{us}}{a G_s + C} \leq x \mid G_s \right] = \mathbb{P}\left[r_{us}^{-\alpha} H_{us} \leq ax + \frac{C x}{G_s} \mid G_s \right] = F_{\tilde{H}_{us}|G_s}\left(ax + \frac{C x}{g_s}\right), \quad (33)$$

where $a = ((U-1)\bar{I} + U\bar{E}_1 + 1)$, $C = \bar{E}_2 + \hat{C}$ and $\tilde{H}_{us} = r_{us}^{-\alpha} H_{us}$. The CDF $F_{\tilde{H}_{us}}(z)$ can be written as (34) where the integral can be solved using [43, Eq. 3.381.8] to obtain (35). In (35), $A = \frac{\beta - \delta}{\eta}$, $V = \frac{\alpha p + 2}{\alpha}$, $\rho = Az$ and $\gamma(\cdot, \cdot)$ is the lower incomplete Gamma function.

Step 2: Similar to the approach followed in the derivation of CM decoding, the MGF of $\gamma_{us}^{(1)}$ conditioned on G_s can be written as

$$M_{\gamma_{us}^{(1)}|G_s}(-t) = 1 - t \int_{x=0}^{\infty} e^{-tx} \left(1 - F_{\tilde{H}_{us}|G_s}\left(ax + \frac{C x}{g_s}\right) \right) dx. \quad (36)$$

Rearranging the terms, (36) can be written as (37). The integral in (37) can be solved using [43, Eq. 6.455.2] to obtain (38),

where

$$v_1(g_s) = A r_{\max}^\alpha \left(a + \frac{C}{g_s} \right), \quad (39)$$

$$v_2(g_s) = A r_{\min}^\alpha \left(a + \frac{C}{g_s} \right), \quad (40)$$

and ${}_2F_1(\cdot)$ is the Gauss hypergeometric function. Since all the S satellites-GS links are independent, the MGF of $\gamma_u^{(1)}$ conditioned on G_s can therefore be written as

$$M_{\gamma_u^{(1)}|G_s}(-t) = \prod_{s=1}^S M_{\gamma_{us}^{(1)}|G_s}(-t). \quad (41)$$

Step 3: Using (20) and averaging over all the G_s , the CDF of $\max_u \gamma_u^{(1)}$ can be derived as

$$F_{\gamma_u^{(1)}}(x) = \int_{g_1} \dots \int_{g_S} \left[\mathcal{L}^{-1} \left\{ \frac{M_{\gamma_u^{(1)}|G_s}(-t)}{t} \right\} (x) \right]^U \times \left\{ \prod_{s=1}^S f_{G_s}(g_s) \right\} dg_1 \dots dg_S. \quad (42)$$

The integral in (42) can be efficiently evaluated using numerical techniques similar to the ones discussed in Appendix D. Thus, using (13) and (42) in (32) with $l = 1$ completes the derivation of the OP in SIC decoding for best user.

V. ASYMPTOTIC ANALYSIS OF OUTAGE PROBABILITY

This section presents the asymptotic analysis to obtain simplified expressions of OP for both CM and SIC-based decoding schemes under the assumption that $\eta_u, \eta_s \rightarrow \infty$.

A. Asymptotic OP for CM-based decoding

Similar to the approach adopted in Section IV-A, the asymptotic CDF $F_{\gamma_{us}}^\infty(x)$ and the MGF $M_{\gamma_{us}}^\infty(-t)$ can be written as

$$F_{\gamma_{us}}^\infty(x) = 1 - \sum_{(k,p,q)} C(k,p,q) \left(1 + \frac{\bar{p}}{\mathcal{I} \eta_{us}} \right) x^{\bar{p}}, \quad (43)$$

$$M_{\gamma_{us}}^\infty(-t) = 1 - \sum_{(k,p,q)} C(k,p,q) \bar{p}! \left(1 + \frac{\bar{p}}{\mathcal{I} \eta_{us}} \right) t^{-\bar{p}}, \quad (44)$$

where

$$C(k,p,q) = \frac{(-1)^q 2 k! \zeta(k) \alpha_{us} \mathcal{I}^{\bar{p}}}{p! q! (\alpha \bar{p} + 2) (\beta - \delta)^{(k+1-\bar{p})}} \times \left(\frac{r_{\max}^{(\alpha \bar{p} + 2)} - r_{\min}^{(\alpha \bar{p} + 2)}}{r_{\max}^2 - r_{\min}^2} \right),$$

$$\mathcal{I} = (U - 1) \mathbb{E}[r_{is}^{-\alpha} |\hat{h}_{us}|^2] + U \sigma_{e_{us}}^2 \mathbb{E}[r_{us}^{-\alpha}],$$

$$a = \eta_u \mathcal{I} + 1 \text{ and } \bar{p} = p + q.$$

A detailed derivation of the above expressions is presented in Appendix E. These expressions are much simpler to comprehend and do not include any integrals. The asymptotic CDF $F_{\gamma_u}^\infty(x)$ and consequently the asymptotic OP $P_{\text{out}}^\infty(\mathcal{R})$

Algorithm 1 OP simulation for CM and SIC

Initialize: No. of channel realizations L
Initialize: U, S, r_{\min}, θ_0 , and other link parameters
Generate: Channel $\mathbf{H}_{U,S,L}, \mathbf{G}_{S,L}, \text{Range } \mathbf{R}_{U,S,L}$
for $l = 1$ to U **do**
 Compute: $\gamma_{us}^{(l)} \quad \forall u \notin \mathbf{D}[l-1]$
 Perform: MRC: $\gamma_u^{(l)} \leftarrow \sum_{s=1}^S \gamma_{us}^{(l)} \quad \forall u \notin \mathbf{D}[l-1]$.
 if $l = 1$ **then**
 CM: $\gamma_u \leftarrow \text{sort } \gamma_u^{(1)}$
 SIC: $\gamma_{\mathbf{D}\{l\}}^{(l)} \leftarrow \max \gamma_u^{(l)}$
 else if $l > 1$ & $\gamma_{\mathbf{D}\{l-1\}}^{(l-1)} > \gamma_{\text{th}}$ **then**
 SIC: $\gamma_{\mathbf{D}\{l\}}^{(l)} \leftarrow \max_{u, u \notin \mathbf{D}[l-1]} \gamma_u^{(l)}$
 else
 SIC: $\gamma_{\mathbf{D}\{l\}}^{(l)} \leftarrow 0$
 end if
 Remove: Entries of $\mathbf{D}[l]$ from \mathbf{H}, \mathbf{G} and \mathbf{R}
end for
Compute: $\mathbb{P}[K_{\text{vis}} \geq S] = 1 - \sum_{j=0}^{S-1} \binom{K}{j} \mathcal{P}^j (1 - \mathcal{P})^{K-j}$
Compute: $\mathbb{P}[\gamma_u \leq \gamma_{\text{th}}] = \text{sum}(\gamma_u^{(l)} \leq \gamma_{\text{th}}) / L$
Compute: $P_{\text{out}}(\mathcal{R}) = \mathbb{P}[\gamma_u \leq \gamma_{\text{th}}] \times \mathbb{P}[K_{\text{vis}} \geq S]$

in scenarios with multiple satellites can therefore be written as

$$F_{\gamma_u}^\infty(x) = \mathcal{L}^{-1} \left\{ \frac{(M_{\gamma_{us}}^\infty(-t))^S}{t} \right\} (x),$$

$$P_{\text{out}}^\infty(\mathcal{R}) = (F_{\gamma_u}^\infty(\gamma_{\text{th}}) \times \mathbb{P}[K_{\text{vis}} \geq S]) + \mathbb{P}[K_{\text{vis}} < S]. \quad (45)$$

It can be observed that at high SNR, the OP attains a floor. It can be attributed to the fact that at high SNR, the performance is limited by the interference and the mismatch due to imperfect CSI such that any further increase in SNR cannot decrease the OP.

The simplified expressions can be used to obtain the optimal number of supported users and the required number of satellites with assured visibility (i.e. the number of satellites S such that $\bar{P}_{\text{vis}}(S) = 1$) for a target OP. The optimization problem can be formulated as

$$\begin{aligned} & \max \quad S \\ & \text{s.t.} \quad \bar{P}_{\text{vis}}(S) = 1, \theta_0 \in [0, 90], \\ & \quad \quad S \in [1, K], S \in \mathbb{Z}^+. \end{aligned}$$

Using the optimized values of satellites S^* and mask angle θ_0^* , the number of supported users can be obtained by solving

$$\begin{aligned} & \max \quad U \\ & \text{s.t.} \quad P_{\text{out}}^\infty(\mathcal{R}) \leq 0.001, \\ & \quad \quad U \geq 1, U \in \mathbb{Z}^+. \end{aligned}$$

The above optimization problems can be solved using a Genetic algorithm (GA) inspired by the natural selection process. It finds optimal or near-optimal solutions by iteratively applying genetic operators such as selection, crossover, and mutation to evolve the population over successive generations. If G represents the maximum number of generations, N represents the initial size of the population, and L represents the size

TABLE III
LIST OF PARAMETERS CONSIDERED FOR SIMULATION

Parameter	Value	Ref.
Mask elevation angle θ_0	10°	
Target rate \mathcal{R}	10 kbps	
Bandwidth B	125 kHz	[3]
User antenna transmit gain	0 dBi	
Satellite antenna Tx/Rx gain	30 dBi	
Constellation Size K	720	
Constellation altitude h	1200 km	
Radius of the Earth r_e	6371 km	[32]
Noise power at the GS σ_w^2	-98 dBm	
Path loss exponent α	2	
Numerical Laplace Inverse	$D = 10, Q = 15$ $\ln(10), N = 21$	[47]
Average Shadowing (m, b, ω)	(2, 0.063, 0.0005)	[48]
Heavy Shadowing (m, b, ω)	(5, 0.251, 0.279)	

of the chromosome (population of candidate solutions), then the upper bound on the time complexity of the entire GA over all iterations can be approximated as $\mathcal{O}(G(N + NL))$. The GA can solve both constrained and unconstrained problems with linear, non-linear and integer constraints. However, for integer constraints, the GA can only find solutions with non-linear inequalities. Hence the assured visibility condition can be approximated and reformulated as $0.999 - \bar{P}_{\text{vis}}(S) \leq 0$. As shown in Section VI, the above simplified expressions can be used to derive interesting insights on the optimal region of operation in terms of the number of devices, satellites, mask angle and constellation size.

Remark (diversity order): Although the OP attains a floor in scenarios with interference and imperfect CSI, the diversity order can be determined for a simpler scenario with perfect CSI and no interference from other users. The OP at high SNR can be approximated as

$$P_{\text{out}}^\infty(\mathcal{R}) = (G_c \eta_{us})^{-d} + O(\eta_{us}^{-d}), \quad (46)$$

where G_c and d denote the cooperation gain and the diversity order, respectively. Here, it is worth mentioning that the CM and the SIC schemes are synonymous with each other under the no-interference scenario. Using (66) with the approximation of $F_{H_{us}}(x)$ as shown in [49], and ignoring the higher order terms, the asymptotic OP under the no-interference scenario can be written as

$$P_{\text{out}}^\infty(\mathcal{R}) = \frac{(\alpha_{us} R_0 \gamma_{\text{th}})^S}{\Gamma(S+1)} \left(\frac{1}{\eta_{us}} \right)^S, \quad (47)$$

where $R_0 = \frac{2}{\alpha+2} \left(\frac{r_{\text{max}}^{(\alpha+2)} - r_{\text{min}}^{(\alpha+2)}}{r_{\text{max}}^2 - r_{\text{min}}^2} \right)$. Hence the proposed topology achieves a diversity order of S and a cooperation gain $G_c = \sqrt[S]{\Gamma(S+1)} (\alpha_{us} R_0 \gamma_{\text{th}})^{-1}$. It is also intuitively verifiable since there are S independent paths between every user and the GS. Also, the term $\sqrt[S]{\Gamma(S+1)}$ indicates that as the number of satellites (S) increases, the cooperation gain G_c grows sublinearly. This suggests that while adding more satellites improves cooperation, the marginal gain diminishes with each additional satellite.

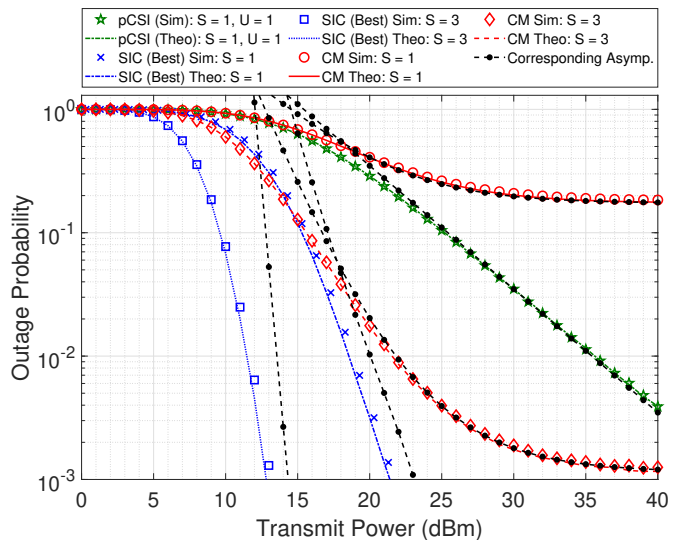


Fig. 5. Validation of theoretical and simulation results: OP vs transmit power P_u in both SIC and CM for $U = 5$ and different number of satellites S . Expressions for no-interference ($U=1$) and perfect CSI (pCSI) are also verified.

B. Asymptotic OP for SIC-based decoding

Since the asymptotic SINR γ_{us}^∞ in (66) is independent of G_s , the asymptotic SINR $\gamma_u^{\infty(1)}$ and consequently the OP $P_{\text{out}}^{\infty(1)}(\mathcal{R})$ for the best user in SIC-based decoding can be conveniently calculated as

$$\begin{aligned} \gamma_u^{\infty(1)} &= \max_u \left(\sum_{u=1}^U \gamma_{us}^\infty \right), \\ P_{\text{out}}^{\infty(1)}(\mathcal{R}) &= F_{\gamma_u^{\infty(1)}}(\gamma_{\text{th}}) \\ &= \left([F_{\gamma_u^{\infty(1)}}(\gamma_{\text{th}})]^U \times \mathbb{P}[K_{\text{vis}} \geq S] \right) + \mathbb{P}[K_{\text{vis}} < S]. \end{aligned} \quad (48)$$

Similar to CM-decoding, the optimal number of supported users and the required number of satellites with assured visibility can be obtained in SIC as well.

VI. RESULTS

This section presents simulation and theoretical results derived in this work to get useful insights into the system. The algorithm for computing OP using Monte-Carlo simulations for both the proposed decoding schemes is provided in Algorithm 1. In this section, initially the theoretical analysis is validated with the simulation results. Later the effect of various system parameters on OP performance is analyzed. Since many parameters affect the performance, an attempt is made to understand them one by one by keeping all other parameters constant. All the simulations and plots have been generated using MATLAB with 10^5 channel realizations. The default parameters used for simulations, unless stated otherwise are mentioned in Table III. The selection of link and stochastic geometry related parameters has been made following 3GPP TR 36.763 [3] and [32], respectively. The imperfect CSI has been modelled using $\chi = 0.05, \phi = 10$ and $\xi = 0.05$ as done in [38]. Also while computing the numerical Laplace inverse as in (26), parameters mentioned in

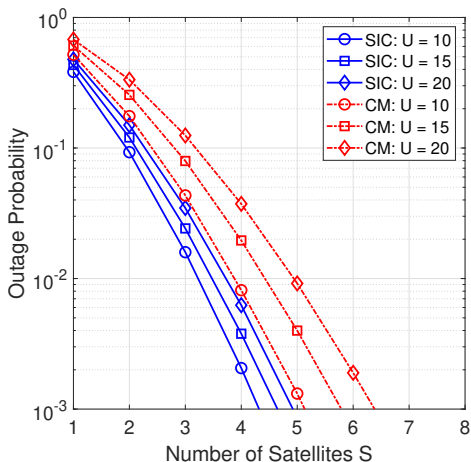


Fig. 6. Effect of number of satellites S : Averaged OP vs S in both SIC and CM at $P_u = 20$ dB and different number of users U .

Table III are used to maintain the discretization and truncation error less than 10^{-10} which is negligible compared to the range of derived OP. For solving the optimization problem using GA in MATLAB, the `ConstraintTolerance`, `FunctionTolerance`, and `PopulationSize` were set to 10^{-6} , 10^{-8} , and 50 respectively. A desktop PC with Intel(R) Core(TM) i7-8700 CPU operating at $3.20 \text{ GHz} \times 6$ cores and 32 GB of memory was utilized for running the solver. The GA algorithm converged in 70 iterations (median of 100 runs), taking 0.2262 sec per iteration on average to obtain the number of satellites S^* and the mask angle θ_0^* . Given S^* and θ_0^* , it converged in 52 iterations (median), taking 4.4152 sec per iteration on average to obtain the maximum number of users U^* .

A. Validation of theoretical and simulation results

Fig. 5 shows the average OP vs transmit power P_u for $U = 5$ users in the case of $S = 1$ and $S = 3$ satellites. The OP for every user in the order of their SINRs has been calculated and then averaged to obtain the average OP of the system. It is observed that the average OP derived theoretically using the approximation is very close to the simulation results for CM decoding and best user in SIC based decoding. This validates the correctness of the derivation presented in Section IV-A and Section IV-B. It can also be observed that the asymptotic curves derived analytically in (45) and (48) approach the simulated curves rapidly, thus validating the correctness of the derived expressions. Moreover, the asymptotic expression presented in (47) for the special case with no interference ($U = 1$) and perfect CSI (pCSI) also matches with the simulations. It can indeed be observed that the slope of the curves is also equal to the number of satellites used for AF ($S = 1$ in this case), thus validating the diversity order as well. Only simulation results are presented in further results to maintain the brevity of the paper.

Two more observations can be made from Fig. 5. First, the OP per user decreases with an increase in transmit power of the IoT users. An IoT user's feasible transmit power range from 12 dB to 20 dB can achieve OP ranging from 10^{-1}

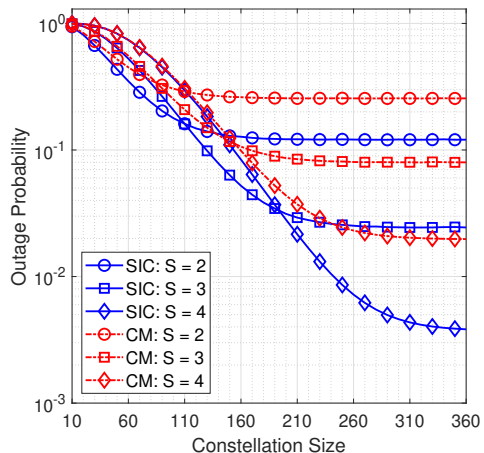


Fig. 7. Effect of constellation size K : OP vs K for both SIC and CM at $P_u = 20$ dB, $U = 15$, and different number of satellites S .

to 10^{-3} in SIC. Second, as the transmit power increases, the interference effect starts dominating, thus leading to the performance difference between SIC and the CM decoding. However, with an increase in the number of satellites, the OP decreases sharply. The scenario with $S = 1$ represents the conventional satellite communication scheme without multiple satellites being visible, unlike the mega-LEO constellations. At high SNRs, the OP in the case of CM decoding decreases from 10^{-1} to 10^{-3} by the addition of two more satellites. It can be observed that by leveraging the benefits of multiple visible satellites, transmit power of 30-35 dB in CM and 12-15 dB for the best user in SIC can achieve an OP of 10^{-3} in a 3 satellite, 5 user system.

B. Effect of the number of satellites S

Fig. 6 shows the OP as a function of number of satellites S for $U = 10, 15$ and 20 users at $P_u = 20$ dBm. It is observed that for a fixed number of users, as the number of satellites increases, the OP decreases sharply. It can be observed that merely an addition of 3-4 satellites can reduce the OP from 10^{-1} to 10^{-3} in both CM and SIC decoding. This also clearly demonstrates how the IoT users can leverage multiple visible satellites of the constellation to enhance system performance. Additionally, it is interesting to note that the OP for 15 users case in SIC is less than the OP for 5 users case in CM.

C. Effect of constellation size K

Fig. 7 shows the effect of the constellation size K on OP for $U = 15$ users at $P_u = 20$ dB, and $S = 2, 3$ and 4 satellites. It can be observed that OP decreases smoothly with an increase in K until a floor is reached. In this case, the floor represents the scenario where OP can't be decreased further, even by adding more satellites to the constellation. The point at which OP saturates denotes the constellation size for which the visibility of S satellites to be utilized in AF-relaying can be ensured (i.e. the constellation size such that $\mathbb{P}[K_{\text{vis}} \geq S] = 1$). Given a target OP to be achieved and the number of satellites intended to be used for AF-relaying, this figure can be utilized to obtain the minimum required size of

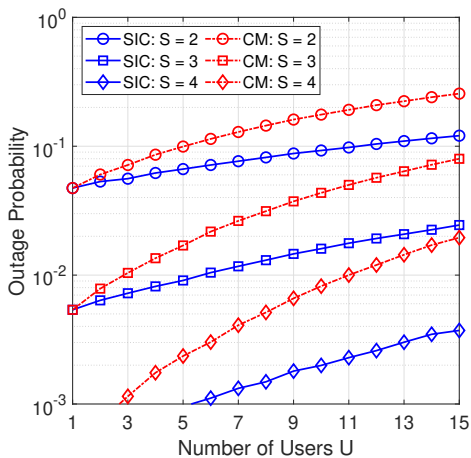


Fig. 8. Effect of number of users U : Average OP vs U for both SIC and CM scheme at $P_u = 20$ dB and different values of satellites S .

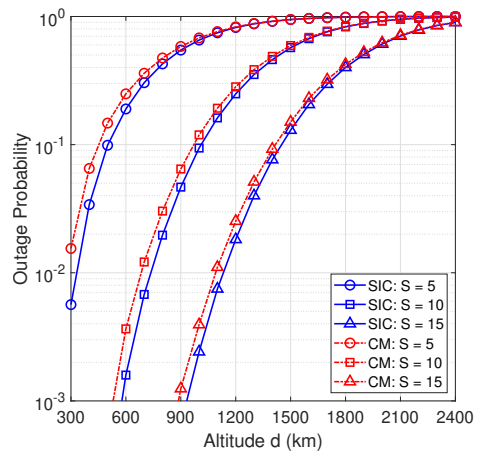


Fig. 9. Effect of altitude d : Average OP vs d for both SIC and CM at $P_u = 20$ dB, $U = 15$ and different values of satellites S .

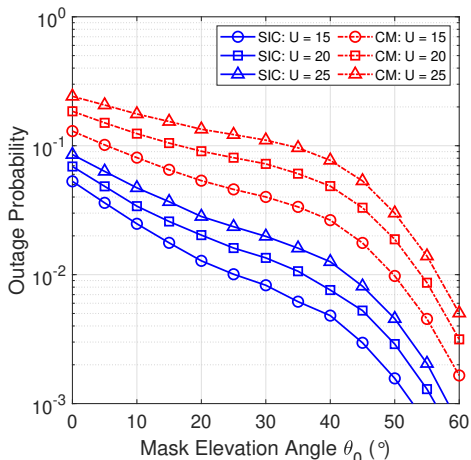


Fig. 10. Effect of mask elevation angle θ_0 : OP vs θ_0 for both SIC and CM at $P_u = 20$ dB, $S = 3$ and different number of users U .

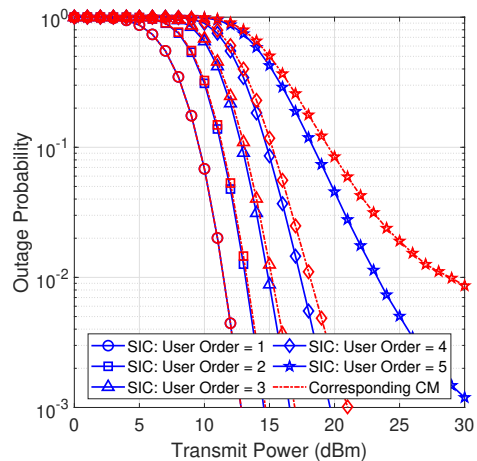


Fig. 11. Effect of decoding order l : OP vs transmit power P_u for ordered decoding in both SIC and CM for $U = 5$ and $S = 3$.

the mega-LEO constellation. For example, if 4 satellites are to be used for AF-relaying, increasing the constellation size from 150 to 360 can improve the OP from 10^{-1} to 3×10^{-3} in the case of SIC decoding and from 10^{-1} to 2×10^{-2} in case of CM decoding. It can also be observed that for a fixed S , the performance difference between SIC and CM increases with an increase in K before saturating. This can be attributed to the fact that the term $\mathbb{P}[K_{\text{vis}} < S]$ in (16) and (32) dominates at low K values irrespective of the decoding schemes. However, as K increases, $\mathbb{P}[K_{\text{vis}} \geq S]$ also increases, making the performance of decoding schemes more evident.

D. Effect of the number of users U

Fig. 8 shows the impact on the OP as a function of number of users U at $P_u = 20$ dBm for $S = 2, 3$ and 4. It can be observed that the OP increases with an increase in the number of users due to the increase in interference. It can also be observed that the performance gap between the SIC and CM also increases with an increase in U . This can be attributed to the fact that the impact of interference decreases with decoding of subsequent users in SIC whereas CM assumes a constant number of interferers for all the

users. It is interesting to note that the difference between the performance of SIC and CM becomes significant as more and more satellites are added to the system.

E. Effect of altitude d

Fig. 9 shows the impact of altitude on the OP for $S = 5, 10$ and 15 satellites and $U = 15$ users at $P_u = 20$ dBm. It can be observed that OP increases as the altitude increases. This is because the constellation's altitude directly impacts the path loss observed by the signals. It can also be observed that while more satellites enhance the OP performance because of better elevation angles, the benefit of adding more satellites diminishes rapidly with increasing altitude. Hence, the number of satellites and the selection of decoding scheme can be traded-off with the altitude and number of users.

Usually, the LEO satellites are considered to be placed between 600 km to 1800 km. Hence for a desired OP at a fixed transmit power, Fig. 9 can be used to determine the minimum number of satellites required in look angle for various constellations at different altitudes. For example, using SIC, in a network of 15 active users, a minimum of 15 satellites at nearly 900 km are required to achieve an OP of

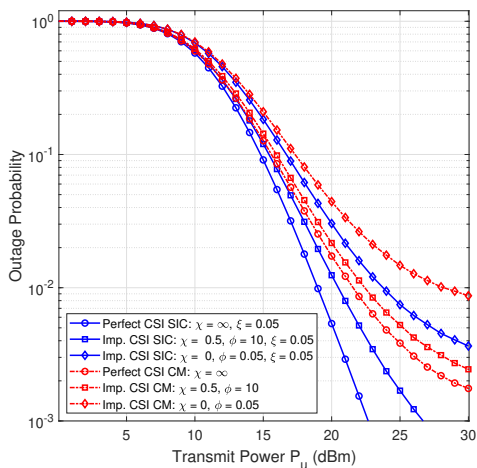


Fig. 12. Effect of imperfect CSI: OP vs SNR plots for scenarios with perfect ($\chi = \infty$) and imperfect CSI in both CM and SIC-based decoding for $U = 5$, $S = 3$ and different values of mismatch parameters χ , ϕ and ξ . Here $\chi = 0$ represents SNR-independent, and $\chi \neq 0$ represents SNR-dependent CSI mismatch.

10^{-3} . A similar performance can be achieved with 10 satellites only if placed at an altitude of 600 km.

F. Effect of mask elevation angle θ_0

Fig. 10 shows the effect of θ_0 on OP for $S = 3$ satellites and $U = 15, 20$ and 25 users at $P_u = 20$ dBm. The OP decreases with an increase in θ_0 ; however, the rate of decrease changes at around $\theta_e = 40^\circ$ for the shown case of $S = 3$. It can be explained by the two-fold impact of θ_0 on the OP. As evident from (50) and (56), A_{vis} decreases with an increase in θ_0 . Hence the probability of seeing a defined number of satellites decreases with an increase in θ_0 for every user. It, therefore, tends to increase the OP. On the other hand, as evident from (63), an increase in θ_0 decreases the distance and, consequently, the average path loss between the users and the satellites. It, therefore, tends to reduce the OP. The impact of reducing path loss dominates nearly till $\theta_0 = 40^\circ$. However, after that, the reduced probability of seeing a defined number of satellites rapidly decreases the OP.

G. Effect of decoding order l and trade-offs

Fig. 11 shows the OP for various users in ordered decoding, where user 1 means the first user being decoded in SIC. Similarly, in a 5-user scenario, user 5 means the last user decoded in SIC. The OP for corresponding CM has also been shown in Fig. 11 where the user order is solely determined by the SINRs without removing interference for any user. It can be observed that the initial few users in the order have similar OP for both SIC and CM. It can be attributed to the fact that the interference in both SIC and CM remains nearly similar for the initial few users. However, for higher order decoding in SIC, the interference decreases significantly due to the subtraction of information signals of the decoded user. This is not the case in CM; decoding of higher order users happens in heavy interference from users with better channel conditions. Hence the difference between the OP performance of SIC and CM increases significantly for higher-order users.

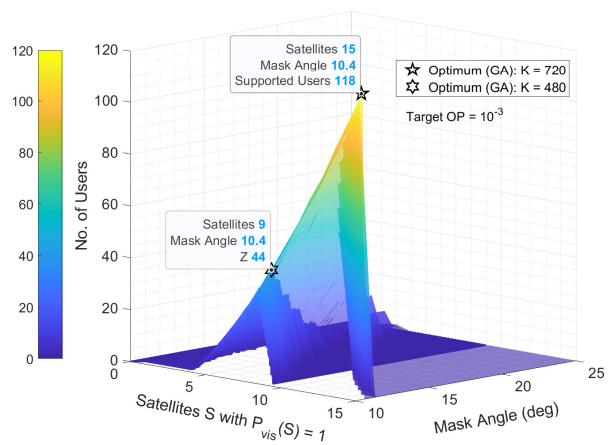


Fig. 13. Maximum number of users which can achieve the target OP of 10^{-3} using CM decoding versus the number of satellites S required with $\bar{P}_{\text{vis}}(S) = 1$ (also mentioned as number of satellites with assured visibility) and varying mask angle. (generated for a constellation of 720 satellites at 1200 km and IoT users with $P_u = 20$ dB)

It can be concluded that trading off with the throughput and desired OP, the initial few users can be decoded using CM only, thus reducing the decoding complexity. However, for applications requiring decoding of all or most users, SIC is preferable to CM.

H. Effect of channel imperfections

Fig. 12 shows the average OP versus the transmit power P_u for both the CM and the SIC-based schemes for $U = 5$ users and $S = 3$ satellites under both perfect and imperfect CSI scenarios. The results demonstrate that the OP performance deteriorates in the presence of CSI mismatch compared to the ideal case when perfect CSI ($\chi = \infty$) is available. Two types of CSI mismatch: the SNR-dependent CSI mismatch ($\chi \neq 0$), and the SNR-independent CSI mismatch ($\chi = 0$) are shown in Fig. 12. When $\chi \neq 0$, the variance of the CSI estimation error depends on the link SNR, and the impact of χ is dominant in determining the system performance. The rate of decline in $\sigma_{e_{u,s}}^2$ and $\sigma_{e_s}^2$ depends on χ , and thus an increase in χ is expected to result in improved OP performance. The SIC decoding is more affected than the CM decoding as the residual error due to imperfect decoding accumulates successively in SIC. For example, at 22dB transmit power, the OP with imperfect CSI at $\chi = 0.5$ is 3.4 times higher than the OP with perfect CSI in the case of SIC decoding but only 1.3 times higher in the case of CM decoding.

In contrast, when $\chi = 0$, the variance of the CSI estimation error solely depends on ϕ . It can be observed that the impact of imperfect CSI is negligible at low SNRs as the products $\eta_{u,s}, \sigma_{e_{u,s}}^2$ and $\eta_{u,s}, \sigma_{e_s}^2$ approach zero, and the CSI quality tends to be perfect. However, as the transmit power increases, particularly above 15 dBm in SIC and 18 dBm in CM decoding, significant degradation in OP performance is observed.

I. Optimum number of users for a target OP

Fig. 13 shows the approximate number of users which can be served for a target OP of 10^{-3} using CM decoding

against the number of satellites with assured visibility and varying mask angles for two different constellation sizes, $K = 480$ and $K = 720$. These results are obtained using the asymptotic expressions derived in Section V. Here, the number of satellites S with assured visibility refers to the number of satellites required such that $\bar{P}_{\text{vis}}(S) = 1$. It can be observed that A_{vis} decreases with an increase in θ_0 , as derived in (50) and (56), thereby decreasing the number of satellites with assured visibility. The maximum number of supported users obtained using the GA optimizer can be verified using a simple grid-based algorithm where the OP is calculated for every possible U for a (θ_0, S) pair obtained from a grid of all likely S, θ_0 values. It is worth mentioning that the asymptotic expressions can be efficiently used for such iterative grid-search methods since they do not contain any integrals to be computed numerically. As shown in Fig. 13, the optimal values obtained from the GA optimizer match the values obtained using the grid search algorithm. For example, considering 720 satellites in the constellation and users with 20 dB transmit power, approximately 118 users can be supported optimally using CM decoding for a target OP of 10^{-3} using 15 satellites at $\theta_0 = 10.5^\circ$. The number of supported users falls down to 44 if the constellation has 480 satellites only. Similar approximations can also be made for SIC decoding.

VII. CONCLUSION

This paper presented a simple and energy-efficient direct-access topology for LEO satellites based IoT networks. The OP performance of the topology was analysed using stochastic geometry to model the random satellite locations. In this context, analytical expressions were derived for average OP in the CM decoding scheme, and the OP of the best user was derived for the SIC decoding scheme, assuming imperfect knowledge of the CSI. Simplified expressions of the OP were also derived under high SNR assumptions which demonstrate that OP attains a floor due to interference and imperfect CSI. The asymptotic expressions were utilized to obtain an optimal region of operation achieving a target OP. Although all the IoT users transmit at the same power, it was found that the SIC decoding scheme performs better than the CM decoding scheme. The theoretical analysis was verified through rigorous simulations. The effects of system parameters like the number of users, number of satellites, altitude, and mask elevation angle of the constellation on the OP performance were discussed in detail. The results of this paper demonstrate that for the practical values of the above system parameters, the proposed topology is feasible and attractive for low-powered IoT networks.

APPENDIX A PROOF FOR CDF AND PDF OF R

The distribution of R can be found in three steps:

- 1) Finding r_{\min} , r_{\max} and the relationship between R and the surface area of the spherical cap, A_{cap} formed by the satellites at the distance less than or equal to R
- 2) Finding the distribution of A_{cap}
- 3) Finding the distribution of R from the distribution of A_{cap}

Step 1: From basic geometry as shown in Fig. 2, $r_{\min} = d$ is the orbital altitude, observed at $\theta_e = 90^\circ$. Also, $r_{\max}(\theta_0)$ will be observed at the mask elevation angle θ_0 . Hereafter it is written as simply r_{\max} to maintain brevity. Applying law-of-cosines for triangles at $\angle XYZ$ gives,

$$(r_e + r_{\min})^2 = r_e^2 + r_{\max}^2 - 2r_e r_{\max} \cos(90 + \theta_0). \quad (49)$$

Solving the quadratic equation (49) for r_{\max} and considering all the distances to be positive, we get

$$r_{\max} = \sqrt{(r_e \sin \theta_0)^2 + (r_e + r_{\min})^2 - r_e^2} - r_e \sin \theta_0. \quad (50)$$

Further derivation to find the relationship between A_{cap} and R can be done on similar lines of [32]. From Fig. 2 where m and n are shown, we can write

$$A_{\text{cap}} = \pi(m^2 + n^2), \quad (51)$$

$$R^2 = (r_{\min} - m)^2 + n^2. \quad (52)$$

Using (51) and (52), we can obtain

$$R^2 = r_{\min}^2 - 2r_{\min}(r_e + r_{\min})(1 - \cos \psi) + \frac{A_{\text{cap}}}{\pi}. \quad (53)$$

Using the geometric identity for surface area of any spherical cap, we can write $A_{\text{cap}} = 2\pi(r_e + r_{\min})^2(1 - \cos \psi)$. Substituting A_{cap} in (53), we get

$$R^2 = r_{\min}^2 + \frac{A_{\text{cap}}}{\pi} \left(1 - \frac{r_{\min}}{r_e + r_{\min}}\right). \quad (54)$$

Similarly at $\theta_e = \theta_0$, a spherical cap of surface area A_{vis} is formed by the all the visible satellites at distance less than or equal to maximum distance r_{\max} from the user. Hence similar to (54), for $R = r_{\max}$, we can write

$$r_{\max}^2 = r_{\min}^2 + \frac{A_{\text{vis}}}{\pi} \left(1 - \frac{r_{\min}}{r_e + r_{\min}}\right), \quad (55)$$

or

$$A_{\text{vis}} = \frac{\pi}{r_e} (r_{\max}^2 - r_{\min}^2) (r_e + r_{\min}). \quad (56)$$

Step 2: From Fig. 2, the CDF of the surface area of the spherical cap formed by satellites at a random distance less than or equal to R from a user is

$$F_{A_{\text{cap}}}(x) = \frac{x}{A_{\text{vis}}}. \quad (57)$$

Step 3: Using the relationship between A_{cap} and R as derived in (54), the CDF of the distance $F_R(r)$ can be written as

$$\begin{aligned} F_R(r) &= \mathbb{P}(R \leq r) = \mathbb{P}(R^2 \leq r^2) \\ &= \mathbb{P}\left(r_{\min}^2 + \frac{A_{\text{cap}}}{\pi} \left(1 - \frac{r_{\min}}{r_e + r_{\min}}\right) \leq r^2\right) \\ &= \mathbb{P}\left(A_{\text{cap}} \leq \frac{\pi(r^2 - r_{\min}^2)}{1 - \frac{r_{\min}}{r_e + r_{\min}}}\right) \\ &= \frac{\pi(r^2 - r_{\min}^2)}{A_{\text{vis}} \left(1 - \frac{r_{\min}}{r_e + r_{\min}}\right)}. \end{aligned} \quad (58)$$

Using (56) in (58), we can write

$$F_R(r) = \frac{r^2 - r_{\min}^2}{r_{\max}^2 - r_{\min}^2}, \quad \text{for } r_{\min} \leq r \leq r_{\max}, \quad (59)$$

where the r_{\max} is given by (50). The corresponding PDF can be found by differentiating (59) with respect to r .

APPENDIX B

PROOF FOR SUCCESS PROBABILITY OF K_{VIS}

The success probability is given by the ratio of the surface area of the spherical cap region where a visible satellite can lie to the total surface area of the sphere. It can be written as

$$\mathcal{P} = \frac{A_{\text{vis}}}{4\pi (r_e + r_{\min})^2}. \quad (60)$$

Using (56) in (60), we can write

$$\begin{aligned} \mathcal{P} &= \frac{\pi(r_{\max}^2 - r_{\min}^2)(r_e + r_{\min})}{4\pi r_e (r_e + r_{\min})^2} \\ &= \frac{r_{\max}^2 - r_{\min}^2}{4r_e (r_e + r_{\min})}. \end{aligned} \quad (61)$$

APPENDIX C

DERIVATION OF $\mathbb{E}[r_{us}^{-\alpha} H_{us}]$

Since H_{us} and R_{us} are independent, $\mathbb{E}[r_{us}^{-\alpha} H_{us}]$ can be written as

$$\mathbb{E}[r_{us}^{-\alpha} H_{us}] = \mathbb{E}[r_{us}^{-\alpha}] \mathbb{E}[H_{us}]. \quad (62)$$

Using (2) and (10), $\mathbb{E}[r_{us}^{-\alpha}]$ and $\mathbb{E}[H_{us}]$ can be solved as

$$\begin{aligned} \mathbb{E}[r_{us}^{-\alpha}] &= \int_{r_{\min}}^{r_{\max}} r_{us}^{-\alpha} f_R(r_{us}) dr_{us} \\ &= \begin{cases} \frac{2(r_{\max}^{2-\alpha} - r_{\min}^{2-\alpha})}{(2-\alpha)(r_{\max}^2 - r_{\min}^2)} & \text{for } \alpha \neq 2, \\ \frac{2}{r_{\max}^2 - r_{\min}^2} \ln\left(\frac{r_{\max}}{r_{\min}}\right) & \text{for } \alpha = 2, \end{cases} \end{aligned} \quad (63)$$

and

$$\begin{aligned} \mathbb{E}[H_{us}] &= \int_0^{\infty} h_{us} f_{H_i}(h_{us}) dh_{us} \\ &= \sum_{\kappa=0}^{m_i-1} \frac{\alpha_i \zeta(\kappa) \eta_i \Gamma(\kappa+2)}{(\beta_i - \delta_i)^{\kappa+2}}. \end{aligned} \quad (64)$$

APPENDIX D

NUMERICAL INTEGRATION IN (23)

The integral term in (23) can be efficiently calculated using the `vpaintegral` function of MATLAB. It uses the global adaptive quadrature technique and variable precision arithmetic to perform the integration. The speed of the execution can be traded-off with the tolerance value. Consider

$$\text{func} = M_{\gamma_{us}|r_{us}}(-t) f_R(r_{us}),$$

where $f_R(r_{us})$ and $M_{\gamma_{us}|r_{us}}(-t)$ are given in (10) and (22), respectively. Then, the integral term in (23) can be evaluated using

$$\begin{aligned} &\text{vpaintegral}(\text{func}, r, r_{\min}, r_{\max}, \dots \\ &\quad \text{'RelTol', } 1e-4, \text{ 'AbsTol', } 0); \end{aligned}$$

where $r_{\min} = r_{\min}$, $r_{\max} = r_{\max}$ and the integration is done for a relative tolerance of 10^{-4} and the option to set the absolute tolerance is turned off.

APPENDIX E

DERIVATION OF ASYMPTOTIC CDF AND MGF OF γ_{us}^{∞}

The end-to-end SINR expression for the CM-based decoding as shown in (6) can be approximated under the assumption $\eta_u, \eta_s \rightarrow \infty$ as

$$\gamma_{us}^{\infty} \approx \frac{r_{us}^{-\alpha} H_{us}}{\sum_{\substack{i=1 \\ i \neq u}}^U r_{is}^{-\alpha} H_{is} + \sum_{u=1}^U \eta_u r_{us}^{-\alpha} \sigma_{e_{us}}^2 + 1}, \quad (65)$$

since at high SNR, the system tends to become limited by interference only. For mathematical tractability, we write $\mathcal{I} = (U-1)\mathbb{E}[r_{is}^{-\alpha} |h_{us}|^2] + U\sigma_{e_{us}}^2 \mathbb{E}[r_{us}^{-\alpha}]$ and $a = \eta_u \mathcal{I} + 1$. Hence γ_{us}^{∞} can be written as

$$\gamma_{us}^{\infty} \approx \frac{1}{a} r_{us}^{-\alpha} H_{us}. \quad (66)$$

Therefore, using the theorem of transformation of random variables, the asymptotic CDF of γ_{us}^{∞} can be computed as

$$\begin{aligned} F_{\gamma_{us}^{\infty}}(x) &= \mathbb{P}\left[\frac{1}{a} r_{us}^{-\alpha} H_{us} \leq x\right] \\ &= \int_{r_{\min}}^{r_{\max}} F_{H_{us}}\left(\frac{ax}{r_{us}^{-\alpha}}\right) f_R(r_{us}) dr_{us} \\ &= F_{\tilde{H}_{us}}(ax), \end{aligned} \quad (67)$$

where $F_{\tilde{H}_{us}}(z)$ is derived in closed form in (35).

By using the series expansion of the lower incomplete Gamma function, $\gamma(\cdot, \cdot)$ as given in [43, Eq. 8.354.1] in the above equation, we get

$$\begin{aligned} &F_{\tilde{H}_{us}}(z) \\ &= 1 - \left\{ \sum_{(k,p,q)} \frac{(-1)^q 2k! \zeta(k) \alpha_{us}}{p! q! (\alpha \bar{p} + 2) (\beta - \delta)^{(k+1-\bar{p})}} \right. \\ &\quad \times \left. \left(\frac{r_{\max}^{(\alpha \bar{p} + 2)} - r_{\min}^{(\alpha \bar{p} + 2)}}{r_{\max}^2 - r_{\min}^2} \right) (z \mathcal{I})^{\bar{p}} \left(1 + \frac{\bar{p}}{\mathcal{I} \eta_{us}} \right) \right\} \\ &\quad + \mathcal{O}\left(\frac{1}{\eta_{us}}\right), \end{aligned} \quad (68)$$

where q is the iterator for the series expansion of $\gamma(\cdot, \cdot)$, $\bar{p} = p + q$ and $\mathcal{O}\left(\frac{1}{\eta_{us}}\right)$ represents the higher order terms of $(1/\eta_{us})$. Since $\eta_u, \eta_s \rightarrow \infty$, the (68) can further be simplified by neglecting the higher order terms to finally obtain (43).

REFERENCES

- [1] R. Lorrain, "LoRa: Delivering internet of things capabilities worldwide," *Inside Out: Semtech's Corporate Blog*, 2022, (Accessed 15 Oct. 2022). [Online]. Available: <https://blog.semtech.com/lora-delivering-internet-of-things-capabilities-worldwide>
- [2] Z. Qu, G. Zhang, H. Cao, and J. Xie, "LEO satellite constellation for internet of things," *IEEE Access*, vol. 5, pp. 18391–18401, 2017.
- [3] 3rd Generation Partnership Project (3GPP); Technical Specification Group Radio Access Network, "Study on NB-IoT/eMTC support for Non-Terrestrial Networks (NTN) (Rel 17)," *TR 36.763*, 2021.

- [4] I. Portillo, B. G. Cameron, and E. F. Crawley, "A technical comparison of three low earth orbit satellite constellation systems to provide global broadband," *Acta Astronaut.*, vol. 159, pp. 123–135, 2019.
- [5] M. Centenaro, C. E. Costa, F. Granelli, C. Sacchi, and L. Vangelista, "A survey on technologies, standards and open challenges in satellite IoT," *IEEE Commun. Surv. Tutor.*, vol. 23, no. 3, pp. 1693–1720, 2021.
- [6] M. Vaezi *et al.*, "Cellular, wide-area, and non-terrestrial IoT: A survey on 5G advances and the road toward 6G," *IEEE Commun. Surv. Tutor.*, vol. 24, no. 2, pp. 1117–1174, 2022.
- [7] S. Kota *et al.*, "Satellite," in *2022 IEEE Future Networks World Forum (FNWF)*, 2022, pp. 1–182.
- [8] J. M. de Souza Sant'Ana, A. Hoeller, R. D. Souza, H. Alves, and S. Montejo-Sánchez, "LoRa performance analysis with superposed signal decoding," *IEEE Wireless Commun. Lett.*, vol. 9, no. 11, pp. 1865–1868, 2020.
- [9] U. Noreen, L. Clavier, and A. Bounceur, "LoRa-like CSS-based PHY layer, capture effect and serial interference cancellation," in *24th Eur. Wireless Conf.*, 2018, pp. 1–6.
- [10] C. C. Chan, B. Al Homssi, and A. Al-Hourani, "A stochastic geometry approach for analyzing uplink performance for IoT-over-satellite," in *IEEE Int. Conf. Commun.*, 05 2022.
- [11] H. Lin, C. Zhang, Y. Huang, R. Zhao, and L. Yang, "Fine-grained analysis on downlink LEO satellite-terrestrial mmwave relay networks," *IEEE Wireless Commun. Lett.*, vol. 10, no. 9, pp. 1871–1875, 2021.
- [12] D.-H. Na, K.-H. Park, Y.-C. Ko, and M.-S. Alouini, "Performance analysis of satellite communication systems with randomly located ground users," *IEEE Trans. on Wireless Commun.*, vol. 21, no. 1, pp. 621–634, 2022.
- [13] N. A. J. Fraire, S. Céspedes, "Direct-to-satellite IoT - a survey of the state of the art and future research perspectives: Backhauling the IoT through LEO satellites," *ADHOC-NOW: Ad-Hoc, Mobile, and Wireless Networks*, pp. 241–258, 2019.
- [14] J. A. Fraire, S. Henn, F. Dovis, R. Garelo, and G. Taricco, "Sparse satellite constellation design for LoRa-based direct-to-satellite internet of things," in *IEEE Global Commun. Conf. GLOBECOM*, 2020, pp. 1–6.
- [15] An ultra-low cost sensor service for small amounts of data, *Lacuna Space*, (Accessed 15 Oct. 2022). [Online]. Available: <https://lacuna.space/>
- [16] Astronode development kit, *Astrocast*, (Accessed 15 Oct. 2022). [Online]. Available: <https://www.astrocast.com/>
- [17] OG2 Satellite IoT modems, *ORBCOMM*, (Accessed 15 Oct. 2022). [Online]. Available: <https://www.orbcomm.com/en/partners/connectivity/satellite/og2>
- [18] X. Lai, W. Zou, D. Xie, X. Li, and L. Fan, "DF relaying networks with randomly distributed interferers," *IEEE Access*, vol. 5, pp. 18909–18917, 2017.
- [19] N. Lamba, A. K. Dwivedi, and S. Chaudhari, "Performance analysis of selective decode-and-forward relaying for satellite-iot," in *2022 IEEE Globecom Workshops (GC Wkshps)*, 2022, pp. 1127–1132.
- [20] K. J. R. Liu, A. K. Sadek, W. Su, and A. Kwasinski, *Cooperative Communications and Networking*. Cambridge University Press, 2008, ch. 4.
- [21] M. R. Bhatnagar and A. M.K., "Performance analysis of AF based hybrid satellite-terrestrial cooperative network over generalized fading channels," *IEEE Commun. Lett.*, vol. 17, no. 10, pp. 1912–1915, 2013.
- [22] D. B. da Costa and S. Aissa, "Performance of cooperative diversity networks: Analysis of amplify-and-forward relaying under equal-gain and maximal-ratio combining," in *2009 IEEE Int. Conf. on Commun.*, 2009, pp. 1–5.
- [23] N. H. Vien and H. H. Nguyen, "Performance analysis of fixed-gain amplify-and-forward relaying with MRC," *IEEE Trans. on Veh. Technol.*, vol. 59, no. 3, pp. 1544–1552, 2010.
- [24] S. S. Soliman, "MRC and selection combining in dual-hop AF systems with Rician fading," in *Int. Conf. on Comput. Eng. & Syst. (ICCES)*, 2015, pp. 314–320.
- [25] A. Iqbal and K. Ahmed, "A hybrid satellite-terrestrial cooperative network over non identically distributed fading channels," *J. of Commun.*, vol. 6, pp. 581–589, 2011.
- [26] H. A. Suraweera, H. K. Garg, and A. Nallanathan, "Performance analysis of two hop amplify-and-forward systems with interference at the relay," *IEEE Commun. Lett.*, vol. 14, no. 8, pp. 692–694, 2010.
- [27] H. A. Suraweera, D. S. Michalopoulos, R. Schober, G. K. Karagiannidis, and A. Nallanathan, "Fixed gain amplify-and-forward relaying with co-channel interference," in *Int. Conf. on Commun. (ICC)*, 2011, pp. 1–6.
- [28] O. Abbasi, A. Ebrahimi, and N. Mokari, "NOMA inspired cooperative relaying system using an AF relay," *IEEE Wireless Commun. Lett.*, vol. 8, no. 1, pp. 261–264, 2019.
- [29] A. Argyriou, "Multi-source cooperative communication with opportunistic interference cancelling relays," *IEEE Trans. on Commun.*, vol. 63, no. 11, pp. 4086–4096, 2015.
- [30] Z. Gao, A. Liu, and X. Liang, "The performance analysis of downlink NOMA in LEO satellite communication system," *IEEE Access*, vol. 8, pp. 93723–93732, 2020.
- [31] X. Li, J. Li, Y. Liu, Z. Ding, and A. Nallanathan, "Residual transceiver hardware impairments on cooperative NOMA networks," *IEEE Trans. on Wireless Commun.*, vol. 19, no. 1, pp. 680–695, 2020.
- [32] N. Okati, T. Riihonen, D. Korpi, I. Angervuori, and R. Wichman, "Downlink coverage and rate analysis of low earth orbit satellite constellations using stochastic geometry," *IEEE Trans. on Commun.*, vol. 68, no. 8, pp. 5120–5134, 2020.
- [33] N. Okati and T. Riihonen, "Nonhomogeneous stochastic geometry analysis of massive LEO communication constellations," *IEEE Trans. on Commun.*, vol. 70, no. 3, pp. 1848–1860, 2022.
- [34] A. Talgat, M. A. Kishk, and M.-S. Alouini, "Stochastic geometry-based analysis of LEO satellite communication systems," *IEEE Commun. Lett.*, vol. 25, no. 8, pp. 2458–2462, 2021.
- [35] A. K. Dwivedi, S. Praneeth Chokkarapu, S. Chaudhari, and N. Varshney, "Performance analysis of novel direct access schemes for LEO satellites based IoT network," in *IEEE 31st Annu. Int. Symp. Pers., Indoor, Mobile, Radio Commun. (PIMRC)*, 2020, pp. 1–6.
- [36] S. Tegos, P. Diamantoulakis, A. Lioumpas, P. Sarigiannidis, and G. Karagiannidis, "Slotted ALOHA with NOMA for the next generation IoT," *IEEE Trans. on Commun.*, vol. 68, no. 10, pp. 6289–6301, 2020.
- [37] Y. Akhmetkaziyeu, G. Nauryzbayev, S. Arzykulov, A. Eltawil, K. Rabie, and X. Li, "Performance of NOMA-enabled cognitive satellite-terrestrial networks with non-ideal system limitations," *IEEE Access*, vol. PP, pp. 1–1, 02 2021.
- [38] Y. Akhmetkaziyeu, G. Nauryzbayev, S. Arzykulov, A. M. Eltawil, and K. M. Rabie, "Cognitive non-ideal noma satellite-terrestrial networks with channel and hardware imperfections," in *2021 IEEE Wireless Commun. and Netw. Conf. (WCNC)*, 2021, pp. 1–6.
- [39] Y. Akhmetkaziyeu, G. Nauryzbayev, S. Arzykulov, K. Rabie, X. Li, and A. Eltawil, "Underlay hybrid satellite-terrestrial relay networks under realistic hardware and channel conditions," in *2021 IEEE 94th Veh. Technol. Conf. (VTC2021-Fall)*, 2021, pp. 1–6.
- [40] Y. Akhmetkaziyeu, G. Nauryzbayev, S. Arzykulov, K. Rabie, and A. Eltawil, "Ergodic capacity of cognitive satellite-terrestrial relay networks with practical limitations," in *2021 Int. Conf. on Inf. and Commun. Technol. Convergence (ICTC)*, 2021, pp. 555–560.
- [41] A. Abdi, W. C. Lau, M. Alouini, and M. Kaveh, "A new simple model for land mobile satellite channels: first- and second-order statistics," *IEEE Trans. Wireless Commun.*, vol. 2, no. 3, pp. 519–528, 2003.
- [42] V. Singh, P. K. Upadhyay, and M. Lin, "On the performance of NOMA-assisted overlay multiuser cognitive satellite-terrestrial networks," *IEEE Wireless Commun. Lett.*, pp. 1–1, 2020.
- [43] I. Gradshteyn and I. Ryzhik, "Tables of integrals, series and products," *New York: Academic Press*, 2000.
- [44] E. Aboutanios, "Frequency estimation for low earth orbit satellites," Ph.D. dissertation, Fac. of Eng. (Telecommun. Group), Univ. of Technol., Sydney, 2002.
- [45] Semtech Corp., *AN1200.22 LoRa Modulation Basics*. Camarillo, CA, USA, 2015, (Accessed 15 Oct. 2022). [Online]. Available: <https://www.frugalprototype.com/wp-content/uploads/2016/08/an1200.22.pdf>
- [46] M. Aldababsa, M. Toka, S. Gökceli, G. Karabulut Kurt, and O. Kucur, "A tutorial on non-orthogonal multiple access for 5G and beyond," *Wireless Commun. Mob. Comput.*, vol. 2018, 06 2018.
- [47] Y.-C. Ko, M.-S. Alouini, and M. Simon, "Outage probability of diversity systems over generalized fading channels," *IEEE Trans. Commun.*, vol. 48, no. 11, pp. 1783–1787, 2000.
- [48] N. I. Miridakis, D. D. Vergados, and A. Michalas, "Dual-hop communication over a satellite relay and shadowed Rician channels," *IEEE Trans. Veh. Technol.*, vol. 64, no. 9, pp. 4031–4040, 2015.
- [49] X. Wu, M. Lin, Q. Huang, J. Ouyang, and A. D. Panagopoulos, "Performance analysis of multiuser dual-hop satellite relaying systems," *EURASIP J. on Wireless Commun. and Netw.*, vol. 2019, no. 1, pp. 1–12, 2019.